Original Article

MOLECULAR METABOLISM

The mitochondrial NAD kinase functions as a major metabolic regulator upon increased energy demand

Hyunbae Kim [1], Zhiyao Fu [1], Zhao Yang [1], Zhenfeng Song [1], El Hussain Shamsa [1], Thangal Yumnamcha [5], Shengyi Sun [1], Wanqing Liu [4], Ahmed S. Ibrahim [5,6], Nathan R. Qi [7], Ren Zhang [1,3,], Kezhong Zhang [1,2,*]**

ABSTRACT

Objective: The mitochondrial nicotinamide adenine dinucleotide (NAD) kinase (MNADK) mediates de novo mitochondrial NADP biosynthesis by catalyzing the phosphorylation of NAD to yield NADP. In this study, we investigated the function and mechanistic basis by which MNADK regulates metabolic homeostasis.

Methods: Generalized gene set analysis by aggregating human patient genomic databases, metabolic studies with genetically engineered animal models, mitochondrial bioenergetic analysis, as well as gain- and loss- of-function studies were performed to address the functions and mechanistic basis by which MNADK regulates energy metabolism and redox state associated with metabolic disease.

Results: Human *MNADK* common gene variants or decreased expression of the gene are significantly associated with the occurrence of type-2 diabetes, non-alcoholic fatty liver disease (NAFLD), or hepatocellular carcinoma (HCC). Ablation of the *MNADK* gene in mice led to decreased fat oxidation, coincident with increased respiratory exchange ratio (RER) and decreased energy expenditure upon energy demand triggered by endurance exercise or fasting. On an atherogenic high-fat diet (HFD), MNADK-null mice exhibited hepatic insulin resistance and glucose intolerance, indicating a type-2 diabetes-like phenotype in the absence of MNADK. MNADK deficiency led to a decrease in mitochondrial NADP(H) but an increase in cellular reactive oxygen species (ROS) in mouse livers. Consistently, protein levels of the major metabolic regulators or enzymes were decreased, while their acetylation modifications were increased in the livers of MNADK-null mice. Feeding mice with a HFD caused S-nitrosylation (SNO) modification, a posttranslational modification that represses protein activities, on MNADK protein in the liver. Reconstitution of an SNO-resistant MNADK variant, MNADK-S193, into MNADK-null mice mitigated hepatic steatosis induced by HFD.

Conclusion: MNADK, the only known mammalian mitochondrial NAD kinase, plays important roles in preserving energy homeostasis to mitigate the risk of metabolic disorders.

Keywords Energy metabolism; MNADK; Mitochondrial metabolism; Acetylation; Metabolic transcription factors; Diabetes; NADK2

1. INTRODUCTION

Dysregulated energy metabolism is intrinsically linked to the development of metabolic disorders, such as non-alcoholic fatty liver disease (NAFLD) and type 2 diabetes mellitus (T2DM). Nicotinamide adenine dinucleotide (NAD) and its phosphorylated form, nicotinamide adenine dinucleotide phosphate (NADP), play essential roles in energy metabolism [1,2]. NAD and NADP are two major players in metabolism as they function as electron carriers in a multitude of redox reactions. NADP(H) is a cofactor for many enzymes, such as dienoyl-CoA reductase (DECR) and alpha-aminoadipic semialdehyde synthase (AASS), which mediate the metabolism of polyunsaturated fatty acids and lysine degradation, respectively [3]. NADPH, the reduced form of NADP, regenerates cellular oxidative defense systems to counteract oxidative damage [4,5]. Mitochondria represent a major source of oxidative stress because the majority of the reactive oxygen species

[1]Center for Molecular Medicine and Genetics, Detroit, MI 48201, USA [2]Department of Biochemistry, Microbiology, and Immunology, Detroit, MI 48201, USA [3]Department of Internal Medicine, Wayne State University School of Medicine, Detroit, MI 48201, USA [4]Department of Pharmaceutical Sciences, Eugene Applebaum College of Pharmacy and Health Sciences, Wayne State University, Detroit, MI 48201, USA [5]Departments of Ophthalmology Visual Anatomical Science and pharmacology, Wayne State University School of Medicine, Detroit, MI 48201, USA [6]Department of Biochemistry, Faculty of Pharmacy, Mansoura University, Mansoura, Egypt [7]Department of Molecular and Integrative Physiology, University of Michigan Medical School, Ann Arbor, MI 48109, USA

*Corresponding author. Center for Molecular Medicine and Genetics, Detroit, MI 48201, USA. E-mail: kzhang@med.wayne.edu (K. Zhang).

**Corresponding author. E-mail: rzhang@med.wayne.edu (R. Zhang).

Abbreviations: MNADK, mitochondrial NAD kinase; CREBH, cAMP-Responsive Element-binding Protein, Hepatic-specific; PPARα, peroxisome proliferator-activated receptor α; PGC1α, peroxisome proliferator-activated receptor gamma coactivator 1α; FA, fatty acids; TG, triglyceride; NAD, nicotinamide adenine dinucleotide; NADP, nicotinamide adenine dinucleotide phosphate; KO, knockout; HFD, high-fat diet; CTL, control; SNO, S-nitrosylation; CLAMS, Comprehensive Laboratory Animal Monitoring System; OCR, oxygen consumption rate; Sirt, Sirtuin; ROS, reactive oxygen species.

Received May 7, 2022 • Revision received July 20, 2022 • Accepted July 25, 2022 • Available online 6 August 2022

https://doi.org/10.1016/j.molmet.2022.101562

(ROS) is generated from the mitochondrial respiratory chain, and NADPH is critical for mitochondrial antioxidant protection.

The human genome encodes two NAD kinases, NADK and MNADK (also known as NADK2), which phosphorylate NAD to generate cytosolic and mitochondrial NADP, respectively (6—10). The MNADK-deficient patients display hyperlysinemia and elevated plasma levels of C10:2 carnitine, due to reduced activity of DECR and AASS, respectively, resulting from reduced mitochondrial NADP(H) [3,6,7]. We generated MNADK knockout (KO) mice and demonstrated that MNADK is required to prevent stress-induced non-alcoholic steatohepatitis (NASH) in mice [8]. MNADK-KO mice phenocopied MNADK-deficient patients by having elevated plasma lysine and carnitine [3,6—8]. Recent studies showed that MNADK is essential for proline biosynthesis in the mitochondria during cell growth, where glutamate is converted to pyrroline-5-carboxylate, which is required for proline biosynthesis, by NADPH-dependent pyrroline-5-carboxylate synthase [9,10].

In this study, we investigated the function and molecular basis by which MNADK regulates metabolic homeostasis by utilizing the MNADK-KO mouse model. MNADK-KO mice exhibited a type-2 diabetes-like phenotype on a high-fat diet (HFD), which is consistent with the link between MNADK variants and type-2 diabetes in humans. MNADK-KO mice had a defect in fat oxidation and thus increased reliance on carbohydrates for energy production in response to increased energy demands triggered by endurance exercise or fasting. We demonstrated that MNADK plays important roles in preserving energy homeostasis and in maintaining insulin sensitivity under metabolic stress and that over-nutrition represses MNADK activity by S-nitrosylation (SNO) modification of MNADK protein in the liver. Our studies define that MNADK, the only known mitochondria NAD kinase in mammals, plays major roles in maintaining metabolic homeostasis and in mitigating metabolic disorders following metabolic challenges.

2. RESEARCH DESIGN AND METHODS

2.1. Materials

Chemicals were purchased from Sigma unless indicated otherwise. The commercially available antibodies were used to detect protein levels of PPARα (Millipore), PGC1α (Santa Cruz), SIRT1 (Abcam), SIRT3 (Abclonal), NAMPT (Abclonal), MNADK (Sigma), P300 (Thermo Fisher) and GAPDH (Sigma) in mouse liver by Western blot or Immunoprecipitation (IP)-Western blot analyses. Polyclonal anti-CREBH antibody was developed in our lab as previously described [11]. Kits for measuring triglyceride (TG) and fatty acid (FA) were from BioAssay Systems (Hayward, CA). The kit for [GSH]/[GSSG] ratio detection was from Abcam.

2.2. Mice and indirect calorimetry

MNADK-KO mice in which exon 6 of the *Mnadk* gene was deleted were previously described [8]. For the diet study, the atherogenic high-fat diet (HFD) (16% fat, 41% carbohydrate, supplied with 0.5% sodium cholate by weight) was from Harlan Laboratories. Indirect calorimetry was used to determine the volume of oxygen consumed (VO_2), carbon dioxide produced (VCO_2), respiratory exchange ratio (RER), energy production, and locomotive activity. VO_2 and VCO_2 were recorded using a Comprehensive Laboratory Animal Monitoring System (CLAMS, Columbus Instruments). VO_2 and VCO_2 were scaled to lean body mass (LBM) determined using an NMR-based analyzer (Minispec LF90II, Bruker Optics, Billerica, MA). Body fat, lean mass, and free fluid were also measured using an NMR analyzer. To measure energy expenditure and fuel preference, the mice were individually placed into the sealed metabolic chambers with free access to food and water using the Comprehensive Laboratory Animal Monitoring System (CLAMS, Columbus Instruments). To measure energy expenditure and fuel preference during endurance exercise, the mice were each placed into the treadmill chambers to acclimate them to the treadmill environment before the study. The study was conducted in an experimentation room set at 20—23 °C with 12-12 h (6:00PM ~ 6:00AM) dark—light cycles. During dark—light cycles, animals were either put on fasting or run on the treadmills one at a time. VO_2 and VCO_2 in each treadmill chamber were sampled continuously every 5 s. The slope of the treadmill was set at 15° to the horizontal. Mice all ran under a ramp protocol with a starting speed of 5 m/min for 5 min, and 9, 12, and 15 m/min for 5 min at each speed, followed by an increment of 2 m/min for every 2 min. RER, an indication of fuel selection between carbohydrates and fats [12,13], was calculated as VCO_2/VO_2. Total energy expenditure, carbohydrate oxidation, and FA oxidation were calculated based on the values of VO_2 and VCO_2 as previously reported [12,14]. Specifically, the rates of glucose oxidation and fat oxidation were calculated as $4.57 \times VCO_2$ (mL/kg mass/h) $- 3.23 \times VO_2$ (mL/kg mass/h) and $1.69 \times VO_2$ (mL/kg mass/h) $- 1.69 \times VCO_2$ (mL/kg mass/h), respectively. Exhaustion was qualified by a mouse sitting on the shocker for 5 consecutive seconds, at which point the shocker was shut off, the treadmill schedule stopped, and 15 min of recovery data was recorded. All animal experiments were performed in accordance with the protocols approved by the Animal Care and Use Committees of both Wayne State University and the University of Michigan.

2.3. Mitochondrial bioenergetic profiles

The mitochondrial bioenergetic profiles of mouse primary hepatocytes were determined by measuring oxygen consumption rates (OCR) using Seahorse technology (XFe96, Agilent Technologies, Santa Clara, CA, USA) as previously described [15]. Briefly, mouse primary hepatocytes (8,000 cells/well) were cultured in a 96-XF tissue culture microplate (Agilent Technologies) using the complete culture media. The Mito-Stress Test was performed with MNADK-KO and WT control primary hepatocytes using a sequential injection of oligomycin (1.5 μM), FCCP (1 μM), and rotenone/Antimycin (1 μM each). Afterward, maximal OCR and spare respiratory capacity as percentages were calculated by the manufacturer's software, Seahorse Wave Desktop Software.

2.4. Biochemical parameters

To determine hepatic TG levels, approximately 30 mg of liver tissue was homogenized in PBS followed by centrifugation. The supernatant was mixed with 10% Triton X-100 in PBS to measure TG or FA levels using a commercial kit (BioAssay Systems). Mouse hepatic TG or FA levels were determined by normalization to the mass of the liver tissue used for measurement of TG levels. Serum insulin concentrations were measured by an ELISA kit (CrystalChem, Chicago, IL). Blood glucose levels were measured using a glucose monitor (glucometer; Bayer, Indianapolis, IN).

2.5. Mitochondria isolation, NADP(H) and NAD(H) quantification, and measurement of NAD kinase activity

Mitochondria were isolated using the Qproteome Mitochondrial Isolation Kit (Qiagen, Valencia, CA) following the manufacturer's instructions. Briefly, 30 mg of liver tissues were homogenized and incubated in lysis buffer with protease inhibitors (supplied by the kit) for 10 min on an orbital shaker at 4 °C. Samples were centrifuged for 10 min at 1000 g at 4 °C, and the supernatant contained the cytosolic fraction. The pellet was then re-suspended in a disruption buffer with protease inhibitors. The lysate was centrifuged for 10 min at 1000 g at

4 °C, and the resulting supernatant was centrifuged at 6000 g at 4 °C to pellet mitochondria. The levels of NADP(H) (total $NADP^+$ and NADPH) and NAD(H) (total NAD^+ and NADH) were determined using a NADP/NADPH colorimetric quantification kit (BioVision) and an NAD/NADH quantification kit (BioVision), respectively. To perform *in vitro* NAD kinase assay [16,17], 10 μg of biologically active mitochondrial or cytosolic protein fraction isolated from MNADK-KO and WT control mouse livers was added into a reaction mixture containing 100 mM Tris—HCl, pH 7.8, 10 mM $MgCl_2$, 10 mM ATP, 5 mM of NAD^+, in a final volume of 100 μL, in triplicates, followed by incubation at 37 °C for 10 min. The reaction containing NAD^+ was terminated by alkalization followed by neutralization. Likewise, mitochondrial and cytosolic fractions of hepatocyte or mouse liver lysates were used to incubate with the above reaction buffer to examine NADK activity. The amounts of NADP(H) were then determined by NADP/NADPH Quantitation Kit according to the manufacturer's instructions (BioVision, CA).

2.6. Adeno-associated virus (AAV) infection

The high-titer and ultra-pure replication-incompetent AAV subtype 8 (AAV8) expressing a human MNADK or its SNO-resistant variant, MNADK-S193, were prepared by Cyagen VectorBuilder (www.vectorbuilder.com). For AAV injection experiments, recombinant AAV8 expressing human MANDK or MNADK-S193 was injected into MNADK-KO mice through tail-vein injection at a dose of 2×10^{11} genome copies (GC) per mouse. Approximately 1×10^{10} PFU of AAV in 0.20 mL of PBS was intravenously injected into a mouse of approximately 20 g of body weight.

2.7. Western blot and co-immunoprecipitation analysis

Equal amounts of denatured mouse liver protein lysates were run on SDS-polyacrylamide gels and then transferred to polyvinylidene difluoride membranes. The blots were incubated with the primary antibody (1:1000 dilution) overnight at 4 °C, and then incubated with a secondary antibody conjugated to horseradish peroxidase (1:10,000) for 1 h at room temperature. For co-immunoprecipitation, 300 μg of protein extracts were incubated with 20 μl of protein A-agarose beads and 3 μg of a primary antibody in a total volume of 500 μl at 4 °C overnight with rotation. After centrifugation, the supernatant containing non-bound protein was removed and added 1 × sample buffer. The eluted proteins were separated by SDS-PAGE for Western blot analysis.

2.8. Dihydroethidium (DHE) fluorescence staining of ROS signals and [GSH]/[GSSG] ratio measurement in mouse liver tissue

Dihydroethidium, an oxidative fluorescent dye, was used to detect superoxide in segments of frozen liver tissue as described previously [18]. Briefly, fresh unfixed segments of liver tissue were frozen in OCT compound, and transverse sections (10 μm) were generated with a cryostat and placed on glass slides. Sections were then incubated in a light-protected chamber at room temperature for 30 min with 10 μmol/L dihydroethidium (Molecular Probes). Images and fluorescent signals were obtained using a Zeiss laser scanning confocal microscope with an excitation wavelength of 488 nm and an emission wavelength of 585 nm. ImageJ software was utilized to quantitatively analyze the DHE fluorescent intensity. Cells of interest and regions of interest (ROI) were selected and measured for mean fluorescence intensity (MFI) as previously described [19]. A region next to the cell or region of interest that has no fluorescence was selected for background MFI measurement. The MFI of an ROI is subtracted by the background MFI: final MFI = MFI of an ROI − MFI of background. The above-mentioned steps for the other cells in the field of view were repeated, and all the finalized MPIs were added up to calculate the corrected total cell fluorescence (CTCF). [GSH]/[GSSG] ratios in livers of MNADK-KO and WT control mice under normal chow or after the atherogenic HFD were measured using a commercial kit from Abcam according to the manufacturer's instructions.

2.9. Biotin switch assay to detect S-nitrosylated MNADK proteins

The liver tissues from MNADK-KO and WT mice fed normal chow or atherogenic HFD for 4 weeks were processed for biotin-switch assays to detect S-nitrosylated MNADK proteins. Biotin switch assays and *in situ* detection of S-nitrosylated proteins were performed as previously described [20—22]. Specifically, with mouse liver tissue sections, free cysteine thiols in mouse liver proteins were blocked by S-methyl-thiolation followed by conversion of SNO signals to thiols via trans-nitrosation with ascorbate and *in situ* labeling by S-biotinylation of the nascent thiols with biotin-HPDP. Biotinylated proteins were labeled using streptavidin conjugated with Alex 488 in liver tissue sections, which were then immunostained for MNADK using the anti-MNADK antibody and an Alex-568 conjugated secondary antibody. The images were observed using Zeiss 700 confocal microscopy. Colocalizations of S-nitrosylated MNADK were quantified using ImarisColoc software (Bitplane) and analyzed by Pearson's correlation coefficient.

2.10. Oil-red O staining

Frozen liver tissue sections were stained with Oil-red O for lipid contents according to a standard protocol [11]. Briefly, the frozen sections (12 μm) from OCT-embedded livers were air-dried, fixed in 10% buffered formalin, and then washed in water. The slides were rinsed in 60% isopropanol and stained in Oil Red O solution. The slides were washed with 60% isopropanol and water, and then mounted in aqueous mounting media before being subjected to microscopic analysis.

2.11. Generalized gene-set analysis

Metabolic Disorders Knowledge Portal (https://hugeamp.org/) was utilized to extract the results of mega-data analyses across multiple human patient datasets. Metabolic Disorders Knowledge Portal output the common variant gene-phenotype associations by aggregating different GWAS for T2D datasets, each of which has *p*-values and betas for single nucleotide polymorphisms (SNPs). Meta-analyze was then performed to produce a single bottom line p-value and beta for each SNP. The MAGMA, a tool for gene analysis and generalized gene-set analysis of GWAS data [23], was finally run to convert the SNP-level statistics into gene-level statistics. The gene-phenotype results were generated by the MAGMA method. The p-values are summaries of the association strength of all SNPs within the specific gene. The numbers of variants correspond to the numbers of SNPs MAGMA examines, and the numbers of sample sizes correspond to the sample sizes output by the MAGMA.

2.12. Statistics

Experimental results are shown as mean ± SEM. The Integrate module in the software Origin (OriginLab, Northampton, MA) was used to calculate the AUC for GTT and ITT data. Mean values for biochemical data from the experimental groups were compared by unpaired 2-tailed Student's *t*-test unless otherwise indicated. The differences were considered statistically significant if $P < 0.05$.

2.13. Data and resource availability

The data sets used and/or analyzed during the current study are available from the corresponding authors upon request.

A

Human MNADK common gene variant associations with major metabolic phenotypes

Phenotype	P-value	Variant (#)	Z-Stat	Sample size
T2 Diabetes	0.017745	27	2.10	437,457
Total MUFAs	0.002718	4	2.78	8,751
Total PUFAs	0.032993	4	1.84	8,751
Total saturated FAs	0.003209	4	2.73	8,750
Fasting insulin	0.003129	2	2.73	10,701
2-hour glucose	0.040683	4	1.74	13,055

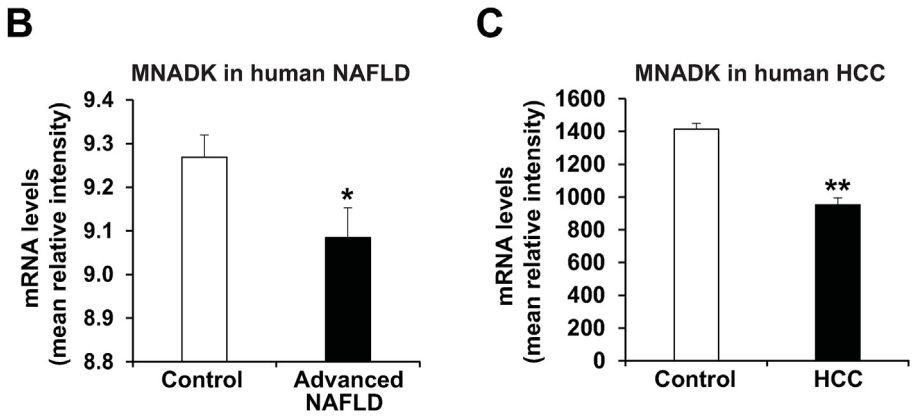

Figure 1: Human *MNADK* gene variants or decreased expression are associated with T2DM, NAFLD, and HCC. (**A**) Human *MNADK* common gene variants are associated with major metabolic phenotypes or disorders. Human *MNADK* gene variants and their association with metabolic phenotypes are determined by generalized gene-set analysis based on the Common Metabolic Diseases Knowledge Portal (CMDKP) comprising of 271 datasets and 330 traits (https://hugeamp.org/). (**B**) Levels of *MNADK* mRNAs in livers of human patients with NAFLD (n = 40 control, 32 advanced NAFLD), based on the datasets of mRNA microarray with human NAFLD or control patient liver biopsy samples (GSE49541 dataset). (**C**) Levels of *MNADK* mRNAs in livers of human patients with HCC (n = 10 control, 81 HCC), based on the datasets of mRNA microarray database with the liver biopsy samples from human HCC or non-tumor control patients (GSE62232). The mean relative intensity based on the mRNA microarray database for each gene is shown. Data are presented as mean ± SEM. Mean values were compared by unpaired 2-tailed Student's *t*-test. *, $P < 0.05$; **, $P < 0.001$).

3. RESULTS

3.1. Human MNADK gene variants or decreased MNADK expression are associated with the incidents of type 2 diabetes mellitus (T2DM), NAFLD, and hepatocellular carcinoma (HCC)

We sought to identify the links between MNADK and major metabolic phenotypes using generalized human gene-set analysis based on the Common Metabolic Diseases Knowledge Portal (CMDKP) comprising 271 datasets and 330 traits (https://hugeamp.org/). In 437,457 human patient samples, 27 *MNADK* gene variants were identified to be significantly associated with T2DM (p value = 0.017745) (Figure 1A). Multi-trait analysis (https://hugeamp.org/gene.html?gene=NADK2) identified that *MNADK* common gene variants were associated with major metabolic phenotypes. Particularly, human *MNADK* common gene variants were associated with the phenotypes of increased fasting insulin and glucose, consistent with MNADK common variant gene-level association with T2DM (Figure 1A). *MNADK* common gene variants were also significantly associated with disorders of total monounsaturated fatty acids (MUFAs), total polyunsaturated fatty acids (PUFAs), and total saturated FAs (Figure 1A). Further, we analyzed the associations of single *MNADK* gene variants with metabolic phenotypes of human patients based on the CMDKP datasets. Single *MNADK* genetic variants are significantly and positively associated with the incidences of type 2 diabetes as well as fasting glucose, MUFA, and PUFA (Supplemental Table 1). These results implicate the functional importance of MNADK in energy metabolism and in the development of metabolic syndrome in humans.

As MNADK is a liver-enriched protein factor [16] (S-Figure 1A—B), we examined the expression profiles of *MNADK* in the livers of patients with NAFLD or HCC based on the National Center for Biotechnology Information Gene Expression Omnibus (GEO) Database (www.ncbi.nlm.nih.gov/geo/). Analysis of the mRNA microarray database of liver biopsy samples obtained from patients with or without NAFLD (GSE49541 dataset) showed that levels of *MNADK* mRNA in the livers of patients with advanced NAFLD were significantly decreased, compared to those in patients with mild hepatic steatosis (Figure 1B). Further, we examined the levels of *MNADK* mRNA in the livers of patients with HCC, a clinical endpoint of NAFLD [24]. Analysis of mRNA microarray database of liver biopsy samples obtained from patients with or without HCC (GSE62232) showed that hepatic levels of *MNADK* mRNA in patients with HCC were significantly decreased, compared to those in patients without HCC (Figure 1C). Additionally, we performed generalized gene-set analysis by aggregating cancer datasets from the Pan-Cancer Atlas of The Cancer Genome Atlas (TCGA) (http://www.cbioportal.org/). Six missense mutations in the human *MNADK* gene were discovered in 377 cases of HCC studied by the TCGA (Firehose Legacy) [25,26], and one missense mutation was identified in 243 cases of HCC studied by (INSERM, Nat Genet 2015) [27]. Kaplan—Meier survival analysis showed that the HCC patients with low MNADK expression displayed less survival probability than the HCC

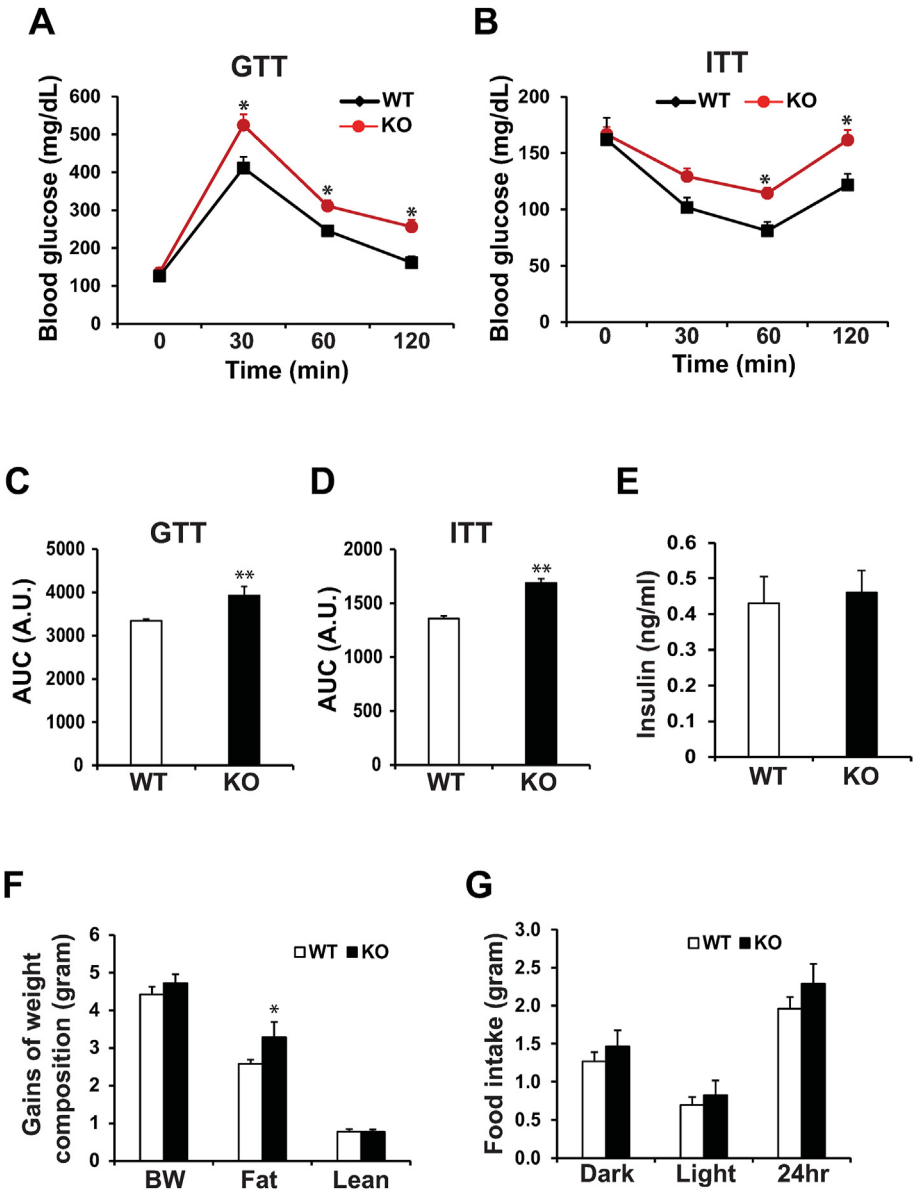

Figure 2: MNADK-KO mice are prone to metabolic syndrome. MNADK-KO and WT control mice were fed with the atherogenic HFD for 3 weeks before being subjected to metabolic phenotyping. (**A-B**) ITT (insulin 1 mU/g body weight after 4h fasting) and GTT (glucose 1.5 g/kg body weight after 14h fasting) with MNADK-KO and WT mice (n = 6). Data are presented as mean ± SEM. Mean values were compared by unpaired 2-tailed Student's *t*-test. *, $P < 0.05$. (**C-D**) The area under curve (AUC) for GTT and ITT of MNADK-KO and WT control mice. The Integrate module in the software Origin (OriginLab, Northampton, MA) was used to calculate the AUC. (**E**) Serum levels of insulin of MNADK-KO and WT mice (n = 6). (**F**) Gains of weights, including body weight (BW), fat mass, and lean mass, of MNADK-KO and WT mice, determined by calculating the increases of body composition mass of the mice after 3-week HFD *vs* before HFD. Data are presented as mean ± SEM (n = 6). *, $P < 0.05$. (**G**) 24h-food intake of MNADK-KO and WT control mice.

patient with high MNADK expression (S-Figure 1D). Although hepatic MNADK protein abundance varies among the HCC patients with different age, gender, and etiological backgrounds, stained MNADK signals in HCC patient liver tissue sections were in general weaker than that of the control liver (S-Figure 1C). Taken together, these data suggest that the *MNADK* gene polymorphism and MNADK suppression are associated with metabolic disorders and HCC malignancy.

3.2. MNADK-KO mice develop insulin resistance and glucose intolerance under overnutrition

To elucidate the function and mechanism by which MNADK regulates metabolism, we first characterized the metabolic phenotype of MNADK-KO mice previously generated in our lab [8]. Western blot analysis confirmed that expression of MNADK is efficiently suppressed in major metabolic tissues, such as the liver, brain, fat, and kidney of MNADK-KO mice (S-Figure 2A). As a liver-enriched protein, expression of both MNADK mRNA and protein was increased in the livers of WT mice upon the fasting challenge (S-Figure 2B—C). MNADK-KO mice had elevated levels of serum lysine and carnitine metabolites, which phenocopied the MNADK-deficient patients that have been identified [3,6—8]. On the normal chow, MNADK-KO mice did not exhibit a distinct metabolic phenotype compared to WT control mice. We then placed MNADK-KO mice with littermate controls on an atherogenic HFD, which contained 16% fat and 41% carbohydrate

supplied with 0.5% sodium cholate. After 3 weeks on the atherogenic HFD, the MNADK-KO mice displayed decreased capability in blood glucose clearance, as shown by the insulin tolerance test (ITT) and glucose tolerance test (GTT) (Figure 2A—D). The phenotypes of insulin resistance and glucose intolerance of the HFD-fed MNADK-KO mice were coincident with increased fat mass gains (Figure 2F, S-Figure 3) but similar levels of blood insulin and food intake, compared to the control mice (Figure 2E,G). These results suggest that MNADK-KO mice are prone to developing a T2DM-like phenotype, which is consistent with the generalized gene-set analysis data for the association of the human *MNADK* common gene variants with T2DM (Figure 1A).

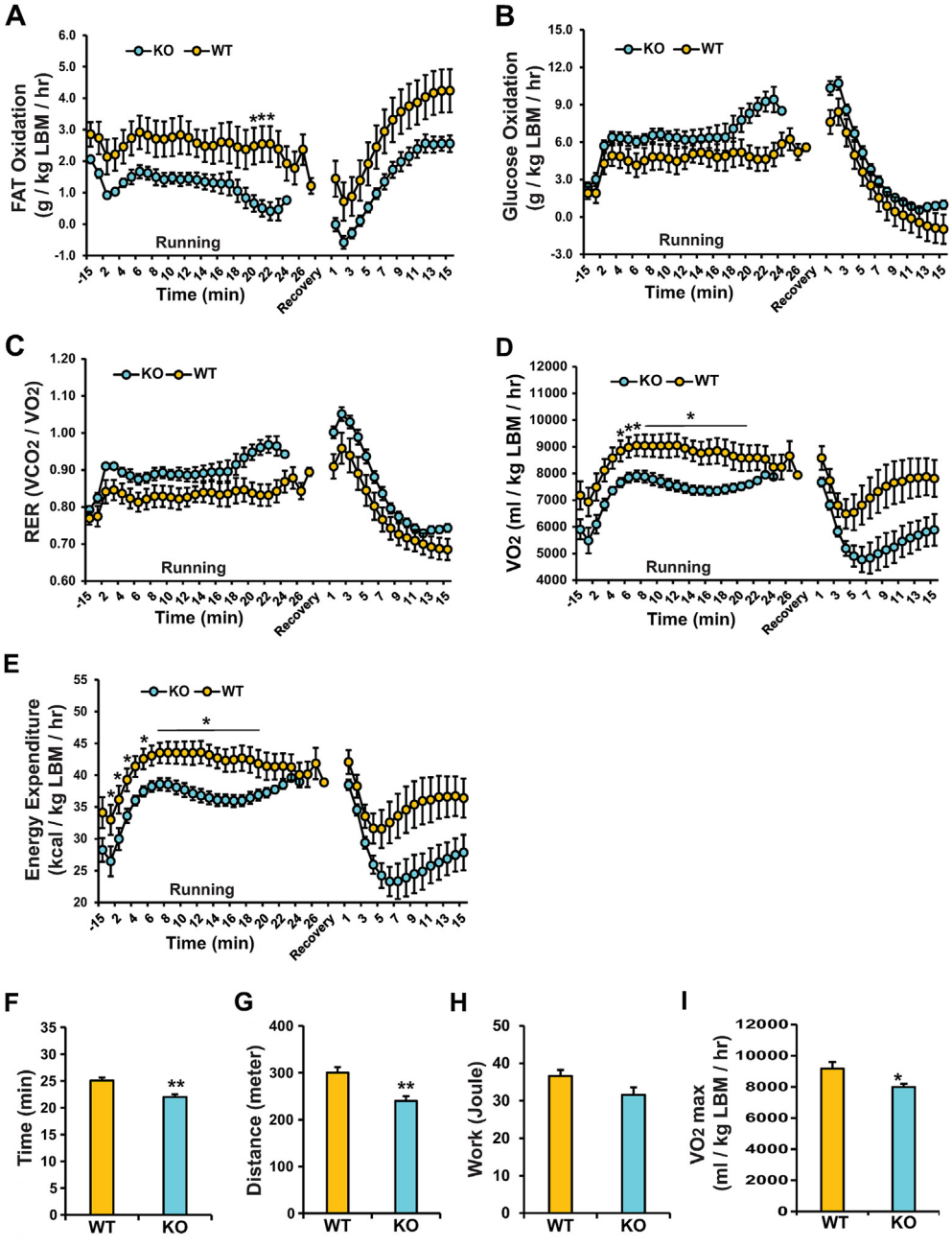

Figure 3: MNADK-KO mice display decreased fat oxidation along with increased RER and decreased energy expenditure in response to endurance exercise. (**A**) Fat oxidation, (**B**) carbohydrate/glucose oxidation, (**C**) RER, (**D**) VO_2, (**E**) energy expenditure, (**F**—**I**) running time (F), distance (G), work joule (H) and VO_2max (I) during an exhaustive treadmill running test for MNADK-KO and WT control mice after HFD, determined by indirect calorimetry using CLAMS. The animals ran on the treadmill, and VO_2 and VCO_2 were monitored continuously. Exhaustion was qualified by a mouse sitting on the shocker for 5 s, at which the shocker was shut off, the treadmill schedule was stopped, and 15 min of recovery data were recorded. VO_2max was defined as a plateau of the oxygen uptake despite increasing running speed. VO_2 and VCO_2 values were normalized to lean body mass (LBM). n = 6 WT or 4 KO male mice. *P $\leq$ 0.05. Data are presented as mean $\pm$ SEM.

3.3. MNADK-KO mice exhibit reduced fat oxidation but increased carbohydrate oxidation along with reduced energy expenditure in response to increased energy demands

To gain insights into the mechanistic basis underlying the metabolic phenotype caused by MNADK deficiency, we tested whether MNADK is required to maintain energy homeostasis through Comprehensive Laboratory Animal Monitor System (CLAMS) studies with MNADK-KO and WT control mice after the atherogenic HFD. Mice were monitored for two days, and VO_2 (oxygen consumed) and VCO_2 (carbon dioxide produced) were measured continuously. With *ad libitum* feeding, MNADK-KO mice were indistinct from WT control mice in energy expenditure. We then examined fat/glucose utilization and total energy expenditure of MNADK-KO and WT control mice under endurance exercise. The animals were placed in the treadmill chambers, and VO_2 and VCO_2 were measured continuously every 5 s. MNADK-KO mice exhibited reduced fat oxidation but increased glucose oxidation, compared to the WT control mice, in response to the treadmill exercise (Figure 3A—B). Consistently, MNADK-KO mice had increased respiratory exchange ratio (RER), an indication of fuel selection between carbohydrate and fat, compared to WT mice, under the endurance exercise (Figure 3C). These results suggest that MNADK-KO mice have a change in fuel selection between fat and glucose, with increased reliance on carbohydrates for energy production, in response to increased energy demands. Further, MNADK-KO mice showed decreased VO_2 levels under the endurance exercise (Figure 3D). Overall, MNADK-KO mice displayed a significant reduction in energy expenditure during the exercise (Figure 3E). Consistently, the MNADK-KO mice exhibited significantly less overall running time and running distance compared to the WT control (Figure 3F—G). Additionally, the MNADK-KO mice had a trend in performing less work ($p = 0.08$) with significantly reduced maximum VO_2 levels (Figure 3H—I). Together, these data suggest that MNADK-KO mice were less efficient in energy expenditure and had a lower running capacity than the WT control mice.

We also examined energy utilization as well as total energy expenditure with MNADK-KO and WT control mice upon nutrient starvation. Consistent with our previous report [8], in response to a 12/12 h light/dark cycle of fasting challenge, MNADK-KO mice exhibited a significant and steady reduction in fat oxidation but elevation in glucose oxidation, compared to the WT control mice (Figure 4A—B). The KO mice displayed increased RER and decreased energy expenditure upon energy demand triggered by fasting (Figure 4C—D). Taken together, these results suggest that MNADK deficiency led to dysregulated energy metabolism, characterized by reduced fat oxidation but increased glucose utilization as well as decreased overall energy production, in response to the increased energy demands triggered by either endurance exercise or fasting. This is consistent with the evidence obtained from generalized gene-set analysis that human *MNADK* common gene variants are significantly associated with the disorders of total MUFAs, PUFAs, and saturated FAs as well as blood glucose levels (Figure 1A).

Further, we profiled mitochondrial bioenergetics of primary hepatocytes isolated from MNADK-KO and WT mice by analyzing oxygen consumption rate (OCR) under stress conditions using Seahorse technology (Figure 4E). During the mitochondrial stress test, the addition of the protonophore uncoupler FCCP (carbonyl cyanide-4 trifluoromethoxy phenylhydrazone) stimulated the OCR to its maximal activity in both WT and MNADK-KO cells, but to a significantly lower extent in MNADK-KO cells (approximately 50% of WT) (Figure 4F). Moreover, the spare respiratory capacity as a percentage and proton leak OCR, but not ATP-linked OCR, of MNADK-KO hepatocytes were significantly reduced, compared to those of WT hepatocytes (Figure 4G—J). Collectively, these results confirmed that MNADK plays an important role in maintaining mitochondrial energy metabolizing capability under stress conditions.

3.4. MNADK deficiency decreases mitochondrial NADP(H) levels and MNADK activity but increases cellular ROS levels in mouse livers on HFD

We sought to understand the mechanistic basis underlying the functional impact of MNADK in energy metabolism. We first examined levels of NADP(H) in the cytosol or mitochondria isolated from MNADK-KO or WT control mouse livers. Consistent with the role of MNADK as a mitochondrial NAD kinase, the levels of mitochondrial NADP(H) in the livers of MNADK-KO mice were significantly reduced, compared to those in WT mice, while the levels of cytosolic NADP(H) were comparable (Figure 5A). To test whether overnutrition impairs MNADK activity in converting NAD to NADP(H) in the liver, we examined NADP(H) levels in the livers of WT mice under normal chow or atherogenic HFD. After 3-week HFD feeding, the levels of mitochondrial NADP(H) in WT mouse livers were significantly reduced (Figure 5B), while the levels of cytosolic NADP(H) in the HFD-fed mouse livers were only marginally changed (Figure 5B), compared to those of the WT mice fed normal chow. Further, mitochondrial and cytosolic protein fractions were prepared from the livers of normal chow- or HFD-fed WT mice, and subjected to quantification of NAD kinase activity using an *in vitro* NAD kinase enzymatic assay method as we previously established [16]. The result showed that NADK activity in mitochondria, but not cytosol, was significantly decreased in the HFD-fed WT mouse livers, compared to that in the normal chow-fed WT mouse livers (Figure 5C), indicating that HFD suppresses MNADK activity in the liver.

NADPH is essential in neutralizing ROS and in regenerating cellular oxidative defense systems to counteract oxidative damage [22,28,29]. We examined ROS levels in the livers of MNADK-KO and WT control mice under normal chow or HFD. Consistent with the reported observations [30,31], HFD increased the levels of ROS, as detected by a fluorescent superoxide probe or dihydroethidium (DHE) staining, in the livers of WT mice (Figure 5D). Interestingly, the amounts of ROS were comparable in the livers of the MNADK-KO and WT mice on a normal chow; on a HFD, however, the KO mice had a significant increase in ROS levels in the liver (Figure 5D). Further, we measured the ratios of [GSH] *vs.* [GSSG] (reduced *vs.* oxidized glutathione), an indicator of cellular oxidative state [32], in the MNADK-KO and WT mice on the normal chow or HFD. Consistent with the increased ROS levels, the ratios of [GSH] to [GSSG] in the livers of HFD-fed MNADK-KO mice were reduced, compared to that in the livers of HFD-fed WT mice (Figure 5E). However, there was no significant change in the [GSH]/[GSSG] ratio in the livers of MNADK-KO mice fed normal chow compared to that in the normal chow-fed WT mice. Together, these results suggest that a decrease in mitochondrial NADP(H), due to MNADK deficiency or HFD (Figure 5A—B), is likely associated with increased cellular ROS levels (Figure 5D). Of note, the redox couple ratio for mitochondrial $NADP^+$/NADPH is an important metabolic parameter indicating mitochondrial energy metabolism and redox state. However, quantitative measurement of compartmental NADPH is technically challenging [33], especially for the current study, as the level of mitochondrial NADP(H) in MNADK KO mouse liver is diminished due to the defect of mitochondrial NADP biosynthesis in the absence of MNADK.

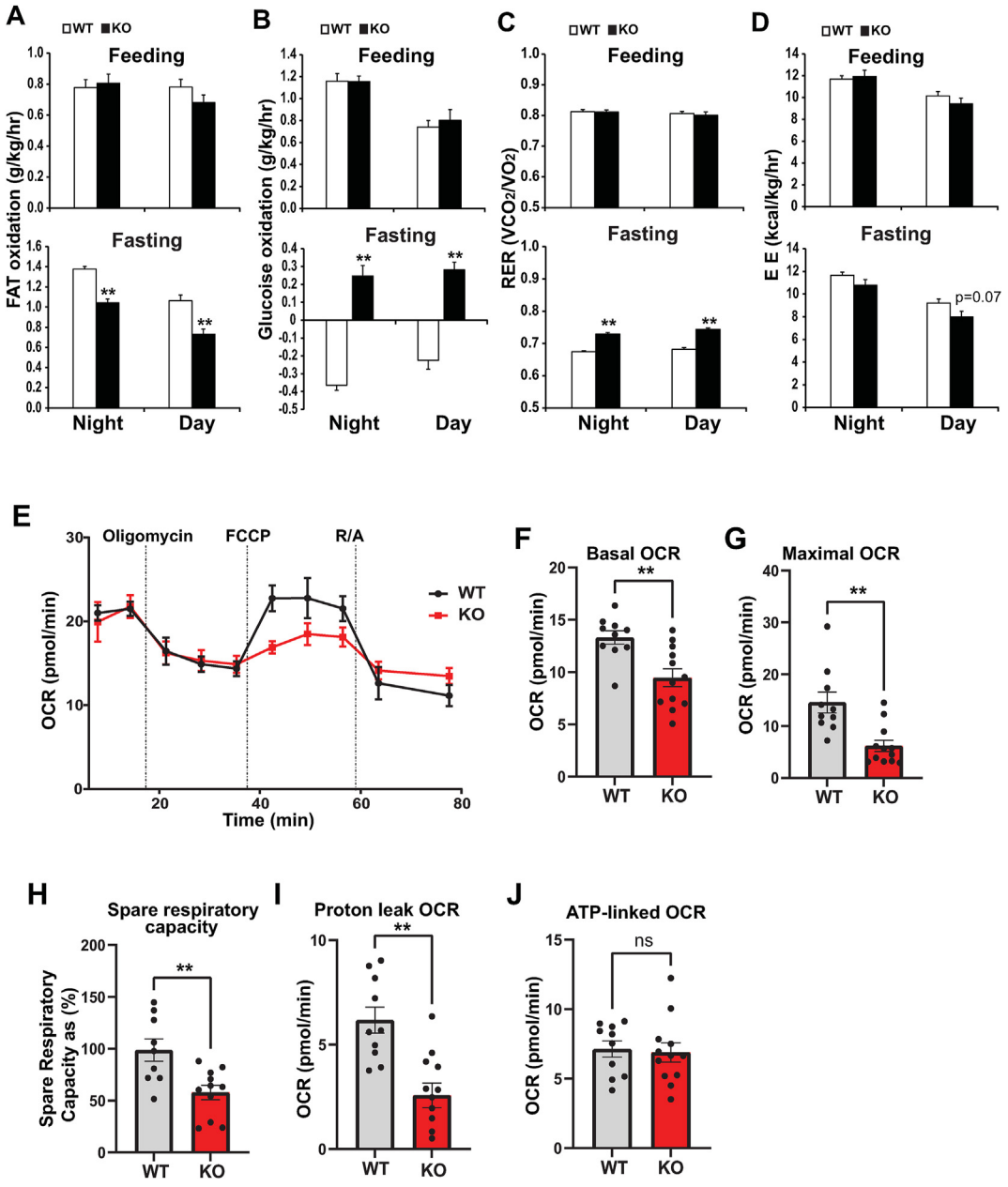

Figure 4: MNADK-KO mice exhibit decreased fat oxidation but increased RER in response to fasting. (**A**) Fat oxidation, (**B**) carbohydrate/glucose oxidation (**C**) RER, and (**D**) energy expenditure (EE) in the HFD-fed MNADK-KO and WT control mice determined by indirect calorimetry using CLAMS. The graphs show quantifications of fat oxidation, carbohydrate oxidation, RER, and energy expenditure in MNADK-KO and WT mice during the nighttime (6 PM–6 AM) and daytime (6 AM–6 PM) under feeding or in response to fasting challenge. Data are presented as mean ± SEM (n = 6 WT or 4 KO male mice). **P ≤ 0.01. (**E-J**) Mitochondrial bioenergetic profiling of MNADK-KO and WT mouse primary hepatocytes. The mitochondrial bioenergetic profiles of hepatocytes were determined by measuring oxygen consumption rate (OCR) using XFe96 Seahorse technology. Mito Stress Test was performed using a sequential injection of oligomycin (1.5 μM), FCCP (1 μM), and rotenone/Antimycin (1 μM each). Basal mitochondrial OCR was normalized by subtracting non-mitochondrial OCR obtained after adding rotenone/Antimycin; R/A, rotenone/Antimycin. Basal OCR (F), Maximal OCR (G), spare respiratory capacity calculated as percentages (H), proton leak OCR (I), and ATP-linked OCR (J) are determined. Seahorse data are presented as mean ± SEM (n = 9–12). **P ≤ 0.01, ns, non-significant.

3.5. MNADK deficiency leads to decreased protein levels but increased acetylation modification of major metabolic regulators or enzymes

NAD(H), NADP(H) and ROS are important signaling messengers that regulate the expression and stability of the key regulators or enzymes of mitochondrial metabolism, such as peroxisome proliferator-activated receptor (PPAR)α and PPARγ coactivator-1 (PGC1)α [34–36]. Increased ROS induced by HFD or obesity is known to destabilize metabolic regulators via proteolysis [34,37]. We wondered whether decreased mitochondrial NADP(H) and increased cellular ROS levels, due to MNADK deficiency and/or HFD (Figure 5A–E), lead to protein instability in MNADK-KO mouse livers. We first examined the expression of the genes encoding the major metabolic transcriptional regulators or enzymes, including Cyclic AMP-responsive element-binding protein 3-like 3, hepatocyte-specific (CREBH) [11], PPARα [38], PGC1α [39], Sirtuin (SIRT)1 [40], SIRT3 [41], and nicotinamide

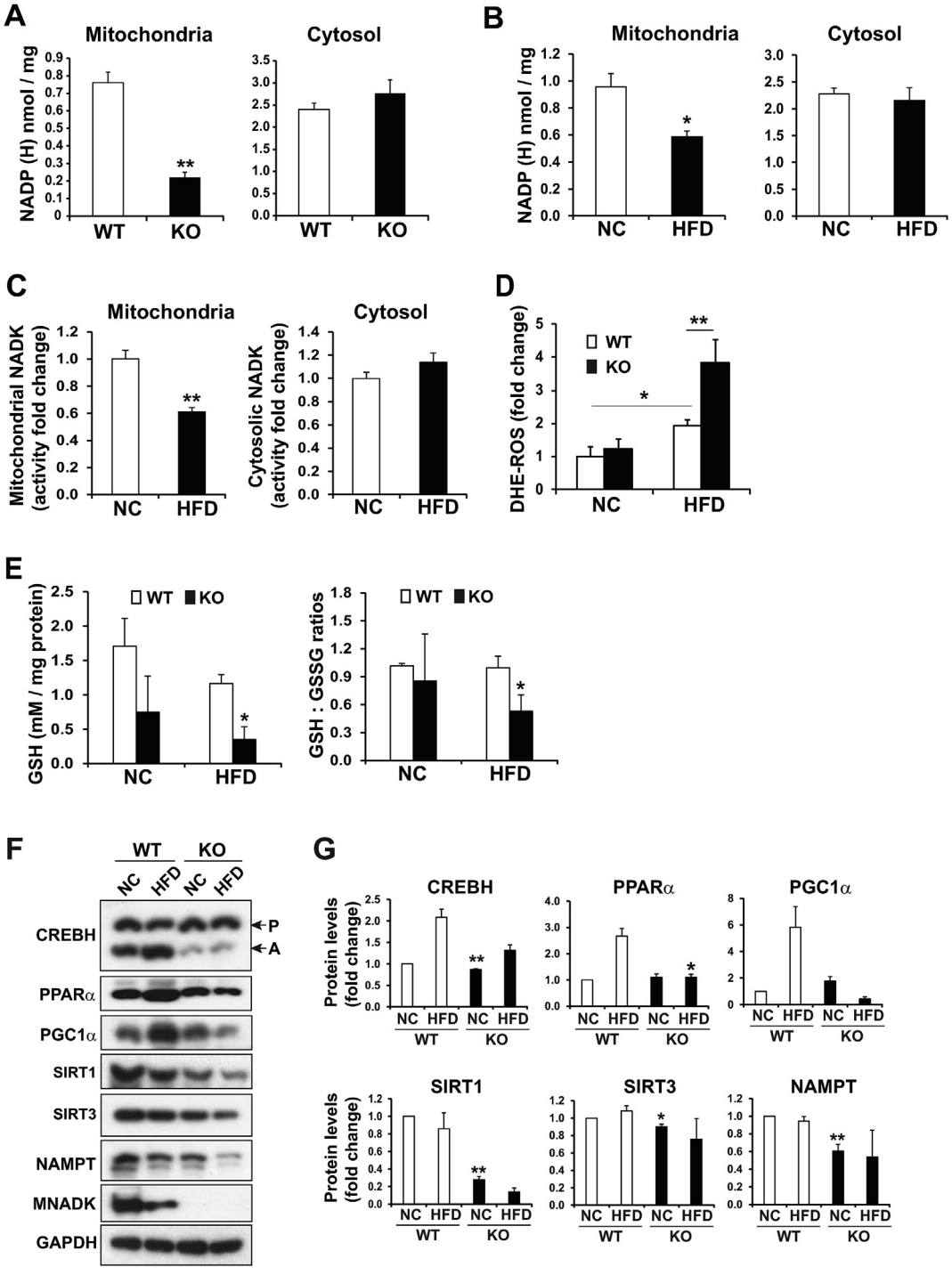

Figure 5: MNADK deficiency leads to decreased mitochondrial NADP(H) levels and MNADK activity, increased cellular ROS, and decreased protein levels of metabolic regulators in mouse livers under the atherogenic HFD for 3 weeks. (**A**) Levels of mitochondrial and cytosolic NADP(H) in the livers of MNADK-KO and WT mice under normal chow (NC). Data are presented as mean ± SEM. $^{**}p \leq 0.01$ (n = 6). (**B**) Levels of mitochondrial and cytosolic NADP(H) in the livers of WT mice under NC or atherogenic HFD. $^{*}P \leq 0.05$ (n = 6). (**C**) Activities of MNADK in the livers of WT mice under NC or HFD. $^{**}p \leq 0.01$ (n = 6). (**D**) Levels of ROS, determined by DHE staining, in the livers of MNADK-KO and WT control mice under NC or HFD. (**E**) [GSH] levels and [GSH]/[GSSG] ratios in the livers of MNADK-KO and WT mice under NC or HFD (n = 3–5 mice per group). [GSH] and [GSH]/[GSSG] ratios were determined by [GSH]/[GSSG] ratio detection assay kit (Abcam, Inc.) (**F-G**) Levels of CREBH (precursor and activated forms), PPARα, PGC1α, SIRT1, SIRT3, NAMPT, MNADK, and GAPDH in the livers of MNADK-KO and WT control mice under NC or HFD, determined by Western blot analyses. The graphs show the fold changes of individual protein levels, determined by Western blot densitometry, in MNADK-KO or WT control mouse livers under NC or HFD. Fold change of the normalized protein levels was calculated by comparing to the level in one of WT mice under NC. The bars denote mean ± SEM (n = 3 experimental replicates). $^{*}P \leq 0.05$, $^{**}P \leq 0.01$.

phosphoribosyltransferase (NAMPT) [42], in the livers of MNADK-KO and WT mice under normal chow or HFD. These stress-inducible metabolic transcriptional regulators or enzymes play major regulatory roles in the energy production pathways, such as mitochondria FA oxidation and TG lipolysis [43,44]. The levels of *Crebh*, *Pparα*, *Pgc1α*, *Sirt1*, *Sirt3*, and *Nampt* mRNAs in the livers of MNADK-KO mice were not significantly changed, compared to those in WT control mouse livers under normal chow or HFD (S-Figure 4). We then examined proteins levels of CREBH, PPARα, PGC1α, SIRT1, SIRT3, NAMPT, and MNADK in MNADK-KO and WT mouse livers. Protein levels of CREBH, PPARα, PGC1α, SIRT1, SIRT3, and NAMPT in MNADK-KO mouse livers were decreased, compared to those in the WT mice (Figure 5F—G). The reduction in protein levels of these metabolic regulators and enzymes was exacerbated in mouse livers under HFD (Figure 5F—G). Moreover, the levels of MNADK protein in the WT mice under HFD were reduced, compared to these of the mice under normal chow (Figure 5F). Additionally, we examined expression of CPT1α and PPARα, the major enzyme and regulator in fatty acid oxidation, in the skeletal muscle of WT and MNADK-KO mice under normal chow or HFD. The levels of muscular CPT1α and PPARα in MNADK-KO mice were significantly reduced, compared to those of WT mice (S-Figure 5A—C), suggesting decreased muscular fatty acid oxidation in MNADK-KO mice. Interestingly, the levels of muscular MNADK in WT mice under HFD were also decreased, compared to those under normal chow (S-Figure 5A,D). Collectively, these results suggested that reduction in protein levels of the major metabolic regulators or enzymes in the absence of MNADK may partially account for decreased fat oxidation and energy consumption as well as type-2 diabetes (Figures 2-3) and hepatic steatosis phenotype [8] in mice on HFD or MNADK deficiency.

Post-translational modification, particularly acetylation or deacetylation, plays a key regulatory role in controlling activities of metabolic regulators [43,45]. Deacetylation, mediated by the NAD-dependent nuclear- or mitochondria-localized deacetylase, is a key regulatory event that enables the activities of metabolic transcription regulators, such as PPARα and PGC1α, in mitochondrial energy metabolism [43,46]. We examined the NAD pool in the livers of WT or MNADK-KO mice under normal chow or the atherogenic HFD. HFD significantly reduced the mitochondrial, but not cytosolic, total NAD [NAD(H)] levels in the livers of WT mice (Figure 6A). Further, hepatic NAD(H) levels were significantly reduced in the MNADK-KO mice compared to those in WT control mice (Figure 6B). These data suggest that MNADK deficiency or HFD leads to decreased mitochondrial NAD pool in the liver. We then examined both acetylation and expression levels of the representative metabolic transcriptional factors, including PPARα, PGC1α, and CREBH, in the livers of MNADK-KO and WT mice under normal chow or HFD. While the levels of PPARα, PGC1α, and CREBH proteins were decreased, lysine-linked acetylation on these proteins in the livers of MNADK-KO or HFD-fed WT mice was significantly increased compared to that in the WT control mice (Figure 6C—D). The increase in acetylation of PPARα, PGC1α, or CREBH protein, due to MANDK deficiency, was further elevated in the liver of the animals under HFD (Figure 6C—D). These results suggest that MNADK impairment, caused by genetic deletion and/or HFD, may decrease PPARα, PGC1α, and CREBH activities through both destabilization and acetylation modification of the proteins. Additionally, we examined protein levels and acetylation modification of P300, a histone acetyltransferase that regulates transcription via chromatin remodeling in the nucleus [47,48], in the livers of MNADK-KO and WT control mice under normal chow or HFD. Both the protein levels and acetylation of P300 in the livers of MNADK-KO mice were significantly higher than those of WT control mice under normal chow or HFD (Figure 6C—D). The differential regulation of P300 vs those (PPARα, PGC1α, and CREBH) involved in mitochondrial energy metabolism, in response to MNADK deficiency, is an interesting question to be investigated in the future.

3.6. HFD compromises MNADK activity by S-nitrosylation (SNO) modification of the protein in mouse livers

SNO, a reversible post-translational modification, represses protein activities through covalent attachment of a nitrogen monoxide group to cysteine residues of target proteins [49]. In obesity or HFD-related overnutrition, chronic metabolic inflammation increases iNOS activity leading to SNO modification of key metabolic regulators in the liver [22,50,51]. To evaluate whether HFD suppresses MNADK activity through SNO, we analyzed the potential of SNO modification on the MNADK proteins of mammalian species. Within the diacylglycerol kinase catalytic pocket of both the human and mouse MNADK proteins, there is a conserved SNO motif, RSEGHLCLPVRYT, characterized by a cysteine (C) residue surrounded by acidic or basic amino acids, where is structurally adjacent to NAD (Figure 7A—B, S-Figure 6). To verify whether overnutrition indeed leads to SNO modification on the MNADK protein in the liver, we utilized a biotin-switch method to label S-nitrosylated proteins in the liver tissue sections of normal chow- or HFD-fed mice, and then examined S-nitrosylated MNADK proteins in the mouse liver tissues by immunofluorescence staining and subsequent quantification analysis [22]. Through this approach, we detected significantly enhanced levels of S-nitrosylated MNADK in the livers of HFD-fed mice compared with the normal chow-fed mice (Figure 7C—D). Additionally, we examined the impact of HFD on the levels of total MNADK protein in mouse livers. Western blot analysis showed that levels of MNADK protein in the livers of HFD-fed WT mice were lower than those of normal chow-fed WT mice (Figure 7E), indicating that the elevation of MNADK protein nitrosylation was not due to a change in protein expression levels. Importantly, the increased levels of S-nitrosylated MNADK protein in HFD-fed mouse livers were correlated with the suppressed MNADK activities (Figure 5C) and reduced levels of mitochondria NADP(H) (Figure 5B) in the livers of HFD-fed mice, suggesting that HFD may compromise MNADK activity through SNO modification of the protein.

We previously demonstrated that MNADK deficiency leads to hepatic steatosis and the associated metabolic phenotypes in mice under the atherogenic HFD [8]. To validate the impact of SNO-mediated repression of MNADK in HFD-induced hepatic steatosis, we evaluated whether expression of an SNO-resistant form of MNADK in MNADK-KO mouse livers can mitigate hepatic steatosis caused by the atherogenic HFD. We generated recombinant adeno-associated virus, subtype 8 (AAV8) over-expressing human MNADK protein (MNADK-WT) or an SNO-resistant form of human MNADK protein (MNADK-S193) (Figure 7F). Both the human and mouse MNADK proteins possess a conserved SNO motif, RSEGHLCLPVRYT, characterized by a cysteine (C) residue surrounded by acidic or basic amino acids (Figure 7A, S-Figure 6). To prevent SNO but maintain the kinase activity of MNADK, we mutated the Cystine residue, C193, within the SNO motif of human MNADK protein to Serine (S193) by changing “TGC” to “AGC”. We injected ultra-pure AAV8 expressing MNADK-WT or MNADK-S193 into MNADK-KO mice through tail-vein injection and then fed the mice with the atherogenic HFD for 4 weeks before euthanizing the mice and analyzing hepatic lipid phenotypes. While expression levels of MNADK or MNADK-S193 in the livers of MNADNK-KO mice receiving AAV8 were comparable (Figure 7G), expression of the MNADK-S193 in the liver significantly decreased the grades of

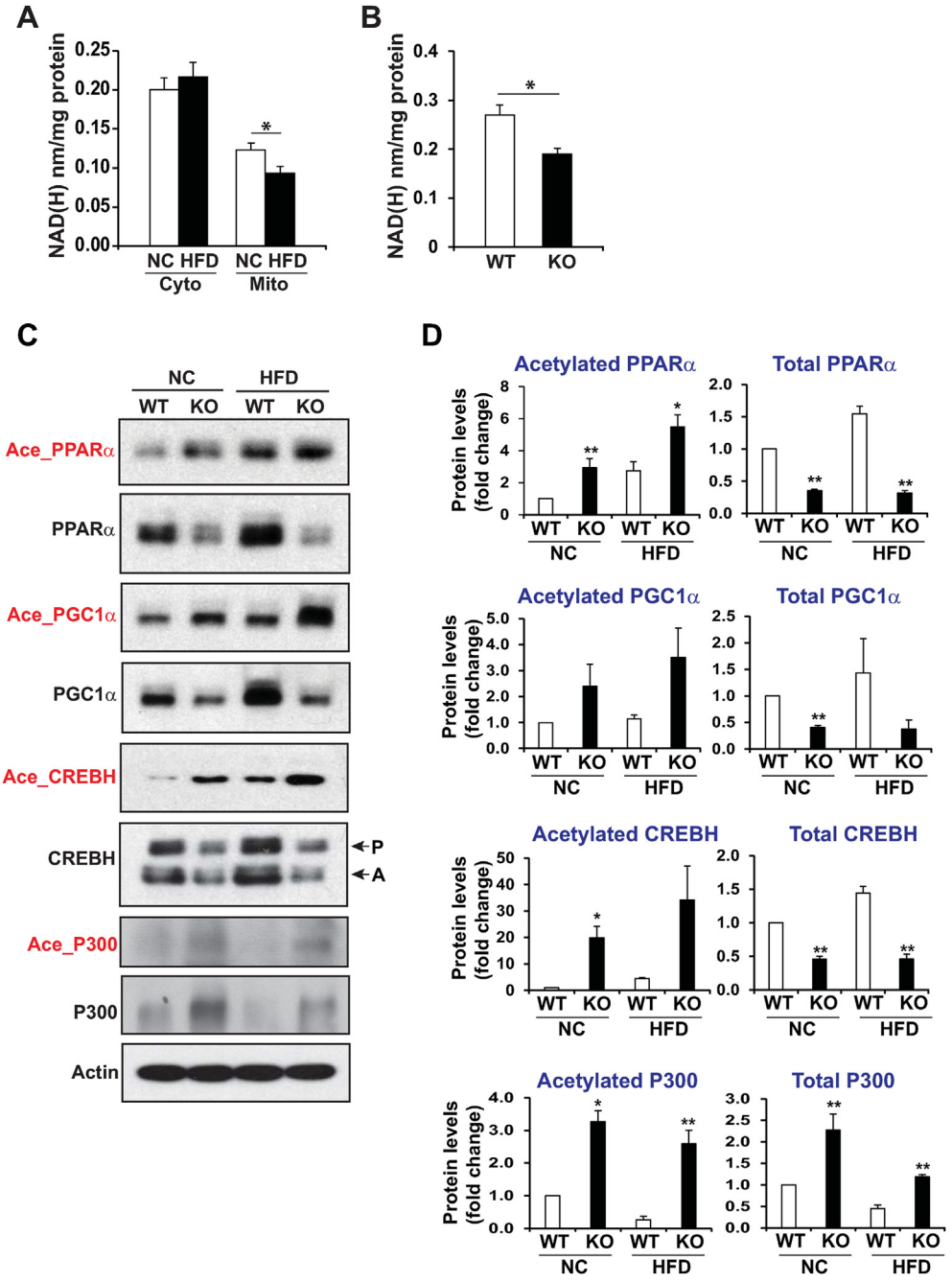

Figure 6: MNADK deficiency leads to increased acetylation but decreased protein levels of metabolic regulators in mouse livers. (**A**) Levels of mitochondrial and cytosolic NAD(H) in the livers of WT mice under normal chow (NC) or atherogenic HFD. Data are presented as mean ± SEM. *P ≤ 0.05 (n = 6). (**B**) Levels of NAD(H) in the livers of MNADK-KO and WT mice. **p ≤ 0.01 (n = 6). (**C**) Acetylated and total protein levels of PPARα, PGC1α, and CREBH in the livers of MNADK-KO and WT control mice under normal chow (NC) or HFD, determined by Western blot analyses. The representative images were shown. (**D**) The graphs show the fold changes of individual acetylated or total protein levels of PPARα, PGC1α, and CREBH, determined by Western blot densitometry, in MNADK-KO or WT mouse livers under NC or HFD. Fold change of the normalized protein levels was calculated by comparing to the level in one of WT mice under NC. The bars denote mean ± SEM (n = 3 experimental replicates). *P ≤ 0.05, **P ≤ 0.01.

hepatic steatosis compared to expression of the MNADK-WT in the MNADK-KO mice under HFD, as shown by oil-red O staining of mouse liver tissue sections (Figure 7H). The quantitative enzymatic assay showed that expression of MNADK-S193 significantly decreased the levels of hepatic TG and FA accumulated in the livers of MNADK-KO mice under HFD (Figure 7I). These results confirmed the impact of SNO-mediated suppression of MNADK in HFD-induced hepatic steatosis and the effect of the SNO-resistant MNADK in mitigating HFD-induced hepatic lipid dysregulation.

To further validate the suppressive regulation of MNADK by SNO modification of MNADK protein, we performed Seahorse analysis with primary hepatocytes isolated from the mice transduced with AAV8 expressing MNADK-WT or MNADK-S193. Over the basal and stress test periods, the primary hepatocytes expressing MNADK-S193 exhibited higher OCRs

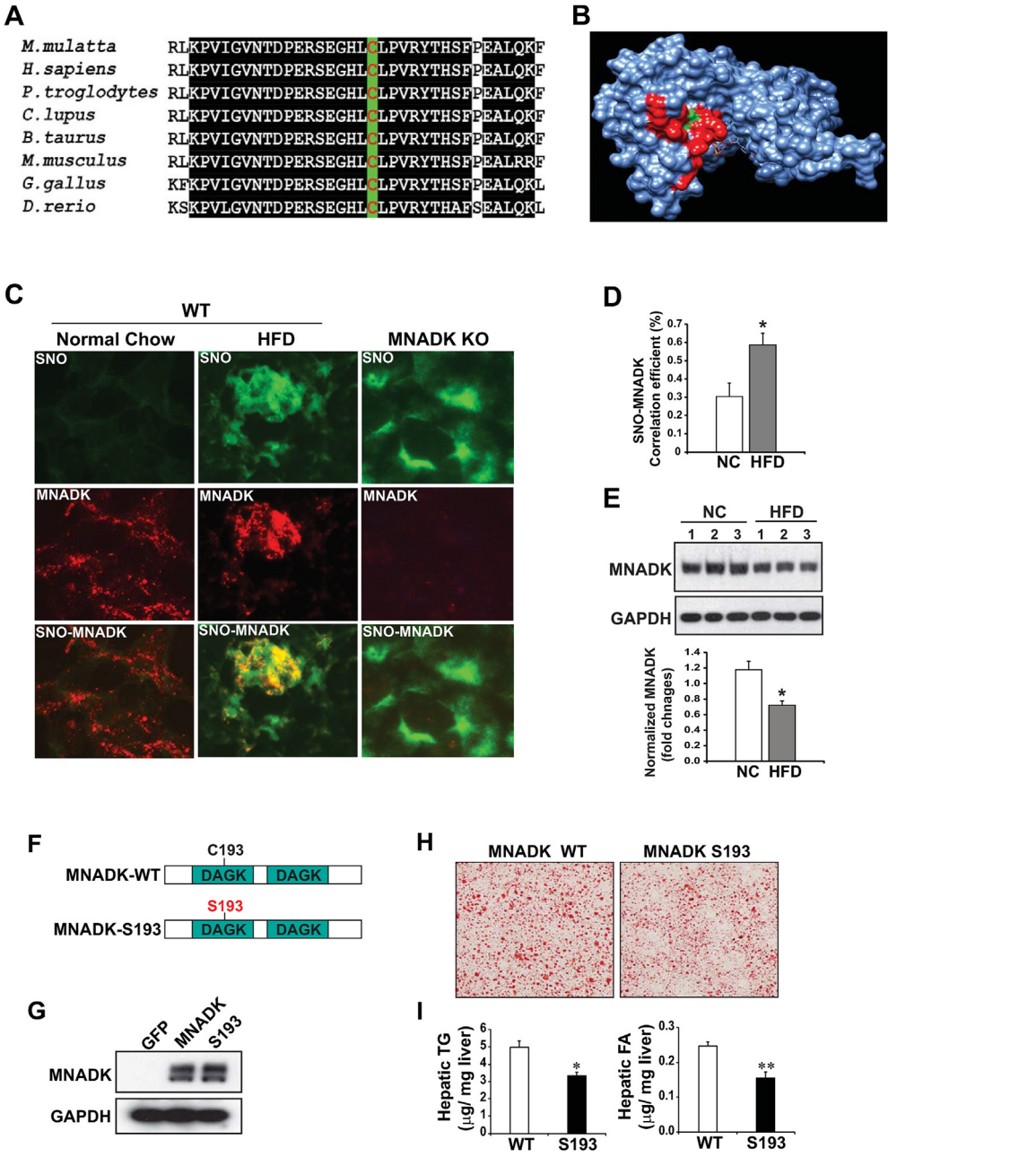

Figure 7: HFD compromises MNADK by S-nitrosylation (SNO) modification of the protein in mouse livers. (**A**) The conserved SNO site within the diacylglycerol kinase catalytic domain of MNADK proteins across the species. (**B**) 3-D structure of human MNADK. NAD^+ (sticks) binds to the catalytic pocket (PDB code: 7N29) [65]. Red denotes the conserved region RSEGHLCLPVRYT, where the Cysteine residue that undergoes SNO is highlighted with green. (**C-D**) Quantitative staining of S-nitrosylated MNADK protein in NC—or HFD-fed mouse livers. Representative images (63 ×) of staining for SNO (green fluorescence) and MNADK (red fluorescence) in the livers from NC- and HFD-fed mice were shown. Panel C shows the quantification of colocalizations (co-efficiency) of SNO-MNADK in the livers of NC- and HFD-fed mice. $^*P < 0.05$ (n = 6). (**E**) Levels of MNADK in the livers of WT mice under NC or HFD, determined by Western blot analyses. The graphs show the fold changes of total MNADK protein, determined by Western blot densitometry, in WT mouse livers under NC or HFD. The bars denote mean ± SEM (n = 3). $^*P \leq 0.05$. (**F**) Domain structure and mutation of SNO-resistant human MNADK variant. DAGK, diacylglycerol kinase domains. (**G**) Expression levels of MNADK in the livers of MNADK-KO mice intravenously injected with AAV8 expressing GFP, MNADK-WT, or MNADK-S193, determined by Western blot analysis. (**H—I**) Oil-red O staining (H) and hepatic TG and FA enzymatic assays (I) with liver tissues of HFD-fed MNADK-KO mice receiving AAV8-MNADK-WT or AAV8-MNADK-S193. Data are presented as mean ± SEM. $^*p \leq 0.05$; $^{**}P \leq 0.01$. (For interpretation of the references to color/colour in this figure legend, the reader is referred to the Web version of this article.)

than the primary hepatocytes expressing MNADK-WT (Figure 8A—F). The addition of the protonophore uncoupler FCCP stimulated the OCR to its maximal activity in MNADK-WT- or MNADK-S193- expressing cells, but to a significantly higher extent in MNADK-S193-expressing cells, with approximately 4-time higher than that of MNADK-WT-expressing cells (Figure 8B,D). Moreover, the spare OCR and ATP-linked OCR were all higher in MNADK-S193-expressing hepatocytes than those in MNADK-WT-expressing hepatocytes (Figure 8E—F). Collectively, these results confirmed that SNO modification of MNADK protein at the residue C193 is a major suppressive regulation of MNADK activity in maintaining

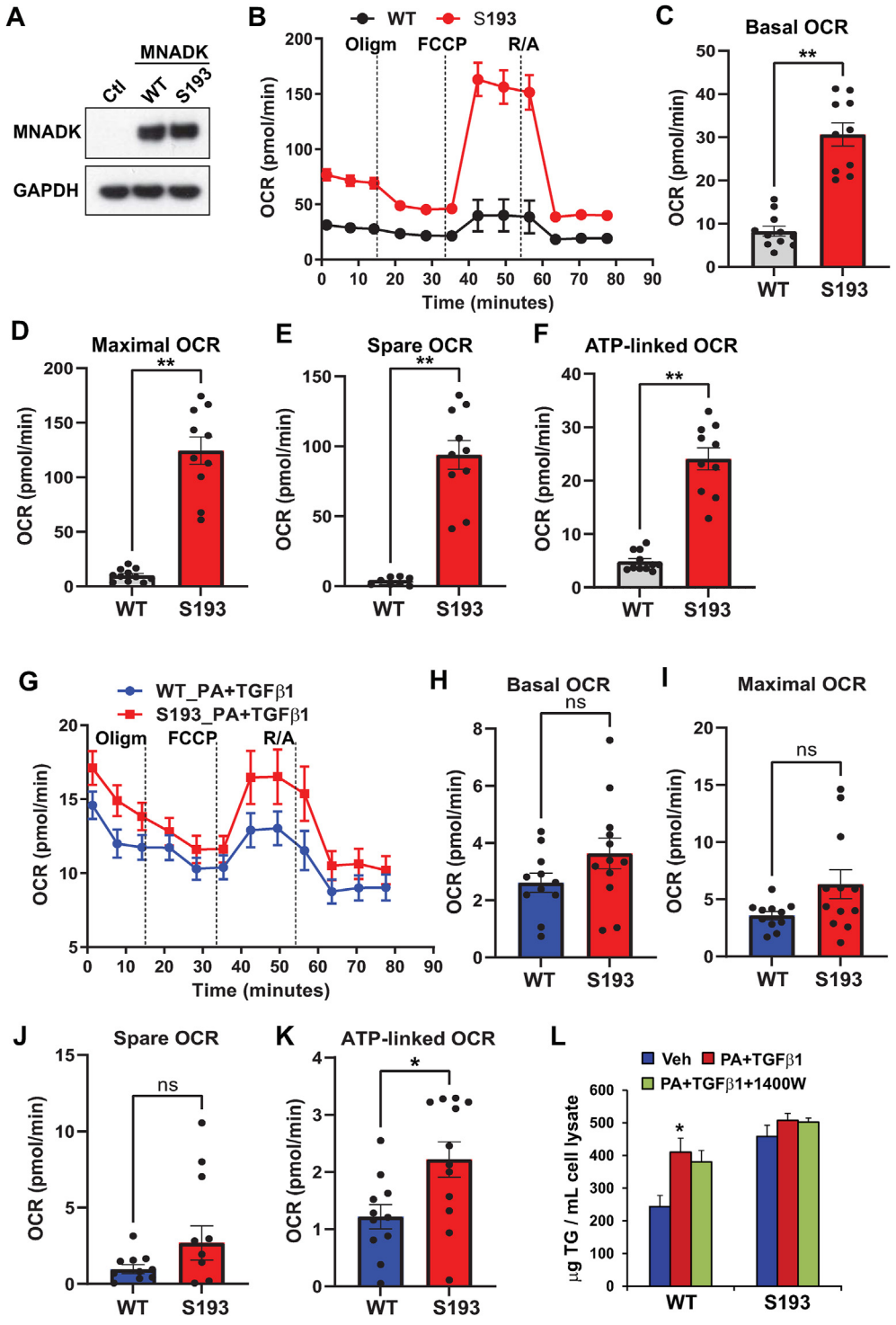

Figure 8: S-nitrosylation (SNO) modification of MNADK protein represents a suppressive regulation of MNADK activity in primary hepatocytes. (**A**) Expression of MNADK in the primary hepatocytes isolated from WT mice intravenously administrated with AAV8 expressing MNADK-WT or MNADK-S193 for 2 weeks, determined by Western blot analysis. Mouse primary hepatocytes expressing LacZ were included as the control. (**B**—**F**) Mitochondrial bioenergetic profiling of primary hepatocytes from WT mice administered with AAV8 expressing MNADK-WT and the SNO-resistant form of MNADK, MNADK-S193, respectively, for 2 weeks, and then subjected to profiling of mitochondrial bioenergetics, within 24-h *in vitro* culture, by analyzing oxygen consumption rates (OCR) using XFe96 Seahorse technology. Mito Stress Test was performed using a sequential injection of oligomycin (1.5 μM), FCCP (1 μM), and rotenone/Antimycin (1 μM each). Basal mitochondrial OCR was normalized by subtracting non-mitochondrial OCR obtained after adding rotenone/Antimycin; R/A, rotenone/Antimycin. Basal OCR (C), Maximal OCR (D), spare OCR (E), and ATP-linked OCR (F) are determined. Seahorse data are presented as mean ± SEM ($n = 12$). $^{**}P \leq 0.01$. (**G-K**) Mitochondrial bioenergetic profiling of primary hepatocytes from WT mice transduced with AAV8 expressing MNADK-WT (WT) or MNADK-S193 (S193) after the treatment of a combination of palmitate (PA) (200 μM) and TGFβ1 (10 ng/mL) for 24 h. Seahorse data are presented as mean ± SEM ($n = 12$). $^{*}P \leq 0.05$; ns, non-significant. (**L**) Levels of TG in mouse primary hepatocytes expressing MNADK-WT or MNADK-S193 treated with PA (200 μM) plus TGFβ1 (10 ng/mL) in the presence or absence of 1400W (40 μM) for 24 h Data are presented as mean ± SEM ($n = 3$ replicates). $^{*}P \leq 0.05$.

mitochondrial energy metabolizing capability, especially under the stress condition. Next, we treated mouse primary hepatocytes expressing MNADK-WT or MNADK-S193 with a combination of palmitate (PA) and TGFβ1 for 24 h to induce hepatic steatosis and injuries as previously described [52,53]. Under the challenge of PA and TGFβ1, MNADK-S193-expressing cells exhibited a trend of higher rates of mitochondrial energy production than MNADK-WT-expressing cells, as shown by the Seahorse analysis (Figure 8G—K). Although MNADK-WT- and MNADK-S193-expressing cells displayed different basal levels of hepatic triglycerides (TG), treatment of a combination of PA and TGF-β1 significantly increased hepatic TG accumulation in the primary hepatocytes expressing MNADK-WT, but not MNADK-S193 (Figure 8L), suggesting the hepatocytes expressing MNADK-S193, the SNO-resistant form of MNADK, are resistant to lipid accumulation induced by PA plus TGFβ1 stimulation. Treatment of 1400W, a specific iNOS inhibitor that can prevent general protein SNO modifications [54,55], insignificantly reduced PA/TGFβ1-induced hepatic TG accumulation in the hepatocytes expressing MNADK-WT, but not MNADK-S193 (Figure 8L). Together, these data support that SNO modification of MNADK represents a suppressive regulation of MNADK activity under the metabolic challenge.

4. DISCUSSION

In this study, we investigated the function and mechanistic basis of the only known mammalian mitochondria NAD kinase, MNADK, in energy metabolism. Our major findings include: 1) Human *MNADK* gene variants or decreased expression of the gene are implicated in type-2 diabetes, NAFLD, and liver cancer; 2) MNADK-KO mice develop insulin resistance and glucose intolerance under overnutrition; 3) MNADK-KO mice exhibit decreased fat oxidation, along with reduced total energy expenditure, in response to increased energy demands triggered by exercise or fasting; 4) MNADK deficiency leads to decreased protein levels but increased acetylation modification of major metabolic regulators or enzymes in the liver; 5) HFD compromises MNADK activity in the liver through SNO modification of the protein; and 6) expression of an SNO-resistant form of MNADK in the liver can mitigate HFD-induced hepatic steatosis. These findings indicate that MNADK is a critical metabolic regulator required to maintain energy homeostasis when the organisms are under metabolic challenges. MNADK not only plays important roles in anti-oxidative protection, but also functions as a key regulator of major metabolic transcriptional regulators or enzymes (Figure 9). Impairment of MNADK, due to genetic variants or overnutrition, may lead to metabolic disorders or malignancy, such as T2DM, NAFLD, and HCC.

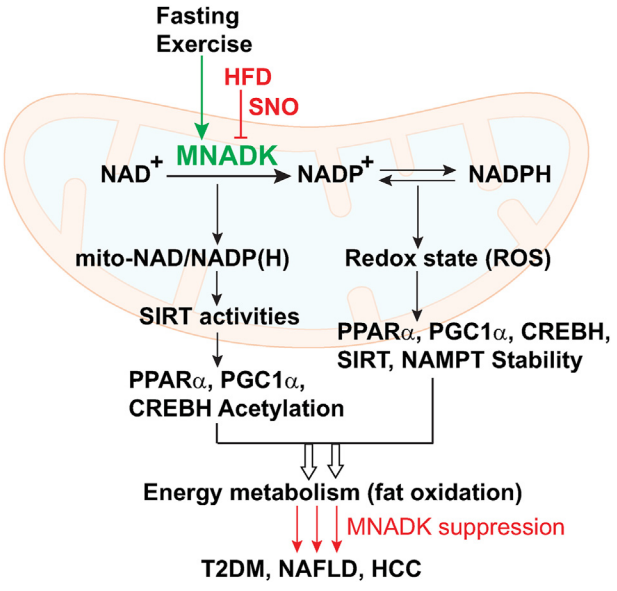

Figure 9: Illustration of the pathways by which MNADK regulates energy metabolism through controlling mitochondrial NADP(H) and cellular ROS. T2DM, type-2 diabetes mellitus; NAFLD, non-alcoholic fatty liver disease; HCC, hepatocellular carcinoma.

As a mitochondrion-localized NAD kinase, MNADK is critical to maintaining energy homeostasis by controlling mitochondrial $NADP^+$ production and redox state. NADPH is essential in neutralizing ROS and regenerating cellular oxidative defense systems to counteract oxidative damages [22,28,29]. NAD, NADP, and ROS can also function as signaling messengers that regulate activities and stability of NAD-dependent metabolic regulators or enzymes, such as PPARα, PGC1α, and SIRTs [35,36,45], and of NADP(H)-dependent mitochondrial enzymes involved in FA metabolism, redox response, and TCA cycle, such as DECR and glutathione-disulfide reductase (GSR) [56,57]. Our studies show that MNADK deficiency led to reductions in mitochondrial, but not cytosolic, NADP(H) as well as increased cellular ROS in mouse livers (Figures 5-6). Compared to the normal chow diet, the atherogenic HFD led to decreased mitochondrial NADP(H) and increased cellular ROS in mouse livers. This is consistent with the finding that HFD compromises MNADK activity in mouse livers (Figure 5C). Importantly, the alterations in mitochondrial NADP(H) and cellular ROS, due to the impairment of hepatic MNADK, lead to decreased protein levels of major metabolic factors in the liver. Protein levels of CREBH, PPARα, PGC1α, SIRT1, SIRT3, and NAMPT in the MNADK-KO mouse livers were decreased compared to those in the WT control mice and this reduction was exacerbated in the livers on HFD (Figure 5F—G). The dysregulated energy metabolism in MNADK-KO mice, characterized by reduced fat oxidation and energy expenditure (Figures 3-4), is partially attributed to the decreased levels of the major metabolic regulators or enzymes in the liver under HFD.

Cellular energy metabolism is closely coupled to the acetylation of metabolic transcriptional activators, such as PPARα and PGC1α, in response to environmental or nutritional signals [43,45,58]. The acetylation status of a protein is the product of the balance between acetylation and deacetylation activities, which is highly dependent on the activities of SIRT deacetylases. SIRTs modify target proteins through their lysine deacetylase and ADP-ribosyltransferase activities [59,60]. While protein levels of PPARα, PGC1α, and CREBH, the major transcriptional activators of energy metabolism, were decreased, acetylation of these proteins in the livers of MNADK-KO or HFD-fed WT mice was significantly increased, compared to that in the control mice (Figure 6). These findings suggest that MNADK impairment, caused by either genetic deletion or HFD-induced SNO modification of the MNADK protein, may decrease the activities of the major metabolic regulators or enzymes through both destabilization and acetylation modification of the proteins. This is also linked to the decreased mitochondrial NAD levels in the liver of HFD-fed WT mice or MNADK-KO mice (Figure 6A—B) because there is a reciprocal regulatory loop between NAD and the major metabolic transcriptional regulators: NAD is required for activation of SIRTs, while SIRTs, PPARα, PGC1α, and CREBH regulate NAD biosynthesis through regulating NAMPT [37]. These multi-layer, reciprocal regulations are critical to maintaining energy homeostasis and shaping metabolic adaptability upon metabolic challenges.

It has been demonstrated that obesity or hepatic steatosis caused by overnutrition or HFD leads to S-nitrosylation (SNO), a dynamic, post-translational modification that represses protein activities, of major

metabolic regulators or enzymes through increased iNOS activity [22,49,50]. Importantly, SNO modification and subsequent functional repression of proteins in cell organelles, such as endoplasmic reticulum (ER), mitochondria, and lysosome, have emerged as important mechanisms by which overnutrition-induced metabolic inflammation dysregulates energy metabolism [22,51]. This is consistent with the view that metabolic syndrome is a degenerative organelle disease characterized by impaired mitochondrial function, defective autophagy, and a dysfunctional ER [50,51,61]. In this study, we show that MNADK is a mitochondrial target of SNO in the liver on HFD (Figure 7). The SNO-caused MNADK impairment may represent a major insult to mitochondria by which HFD dysregulates energy metabolism. Interestingly, we demonstrated that expression of an SNO-resistant form of MNADK in mouse livers could mitigate HFD-induced hepatic lipid accumulation (Figure 7F—I), highlighting that boosting MNADK activity in the liver may represent a novel preventive or therapeutic strategy for lipid-associated metabolic diseases caused by overnutrition.

In summary, our studies suggest that MNADK plays critical roles in preserving mitochondrial function and regulating energy metabolism by controlling mitochondrial NADP(H) biosynthesis and by regulating acetylation states of major mitochondrial regulators or enzymes that shape metabolic adaptability upon metabolic challenges. Our findings have wide implications, given that NADP(H) is involved in a wide array of critical cellular processes, including mitochondrial FA oxidation, TCA cycle, gluconeogenesis, and antioxidant protection. While mouse MNADK is highly enriched in the liver [16], the activities of MNADK in the other metabolic organs may also contribute to the whole-body metabolism. Particularly, muscular MNADK may contribute to the regulation of whole-body energy metabolism, especially under exercise challenges. Pancreatic MNADK may also regulate insulin response, given the important roles of NADPH in pancreatic beta-cell physiology [62]. In the brain, malfunction of hypothalamic mitochondria, due to NADPH deficiency [63,64], may partially contribute to the metabolic phenotypes, such as weight difference and insulin resistance, observed in MNADK-KO mice. Further research on MNADK will provide significant insights into the pathophysiology of several diseases, including metabolic disease, cardiovascular disease, neurodegenerative disease, and cancer, whose pathogenesis mechanisms involve damages by oxidative stress.

AUTHOR CONTRIBUTIONS

KZ and RZ designed and conducted the experiments, analyzed the data, and wrote the manuscript; HK, ZF, ZY, ZS, EHS, TY, ASI, and NRQ performed the experiments, acquired the data, and analyzed the data; SS and WL provided key reagents or critical comments.

DATA AVAILABILITY

Data will be made available on request.

ACKNOWLEDGEMENTS

Portions of this work were supported by National Institutes of Health (NIH) grants DK090313 and DK126908 (to KZ); DK132065 (to RZ and KZ); R01HL134787 (to RZ); R01DK128077 (to SS); DK106540 and DK124612 (to WL); a Pilot and Feasibility Grant (to HK) from the Michigan Diabetes Research Center (NIH Grant P30-DK020572); DK089503 to the Michigan Nutrition and Obesity Research Center; American Heart Association (AHA) grant 18CDA34080403 and NIH core grant P30EY004068 (to ASI); and U2C-DK110768 to the University of Michigan Mouse Metabolic Phenotyping Center.

CONFLICT OF INTEREST

All authors (HK, ZF, ZY, ZS, EHS, TY, SS, WL, ASI, NRQ, RZ, and KZ) have no financial, professional, or personal conflict related to this work to declare.

APPENDIX A. SUPPLEMENTARY DATA

Supplementary data to this article can be found online at https://doi.org/10.1016/j.molmet.2022.101562.

ABBREVIATIONS

MNADK	mitochondrial NAD kinase
CREBH	cAMP-Responsive Element-binding Protein, Hepatic-specific
PPARα	peroxisome proliferator-activated receptor α
PGC1 α	peroxisome proliferator-activated receptor gamma coactivator 1α
FA	fatty acids
TG	triglyceride
NAD	nicotinamide adenine dinucleotide
NADP	nicotinamide adenine dinucleotide phosphate
KO	knockout
HFD	high-fat diet
CTL	control
SNO	S-nitrosylation
CLAMS	Comprehensive Laboratory Animal Monitoring System

REFERENCES

[1] Williamson, D.H., Lund, P., Krebs, H.A., 1967. The redox state of free nicotinamide-adenine dinucleotide in the cytoplasm and mitochondria of rat liver. Biochemical Journal 103(2):514—527.

[2] Imai, S., Armstrong, C.M., Kaeberlein, M., Guarente, L., 2000. Transcriptional silencing and longevity protein Sir2 is an NAD-dependent histone deacetylase. Nature 403(6771):795—800.

[3] Houten, S.M., Denis, S., Te Brinke, H., Jongejan, A., van Kampen, A.H., Bradley, E.J., et al., 2014. Mitochondrial NADP(H) deficiency due to a mutation in NADK2 causes dienoyl-CoA reductase deficiency with hyperlysinemia. Human Molecular Genetics 23(18):5009—5016.

[4] Circu, M.L., Aw, T.Y., 2010. Reactive oxygen species, cellular redox systems, and apoptosis. Free Radical Biology and Medicine 48(6):749—762.

[5] Pollak, N., Niere, M., Ziegler, M., 2007. NAD kinase levels control the NADPH concentration in human cells. Journal of Biological Chemistry 282(46):33562—33571.

[6] Tort, F., Ugarteburu, O., Torres, M.A., Garcia-Villoria, J., Giros, M., Ruiz, A., et al., 2016. Lysine restriction and pyridoxal phosphate administration in a NADK2 patient. Pediatrics 138(5).

[7] Pomerantz, D.J., Ferdinandusse, S., Cogan, J., Cooper, D.N., Reimschisel, T., Robertson, A., et al., 2018. Clinical heterogeneity of mitochondrial NAD kinase deficiency caused by a NADK2 start loss variant. American Journal of Medical Genetics, Part A 176(3):692—698.

[8] Zhang, K., Kim, H., Fu, Z., Qiu, Y., Yang, Z., Wang, J., et al., 2018. Deficiency of the mitochondrial NAD kinase causes stress-induced hepatic steatosis in mice. Gastroenterology 154(1):224—237.

[9] Zhu, J., Schworer, S., Berisa, M., Kyung, Y.J., Ryu, K.W., Yi, J., et al., 2021. Mitochondrial NADP(H) generation is essential for proline biosynthesis. Science 372(6545):968—972.

[10] Tran, D.H., Kesavan, R., Rion, H., Soflaee, M.H., Solmonson, A., Bezwada, D., et al., 2021. Mitochondrial NADP(+) is essential for proline biosynthesis during cell growth. Nat Metab 3(4):571–585.
[11] Zhang, C., Wang, G., Zheng, Z., Maddipati, K.R., Zhang, X., Dyson, G., et al., 2012. Endoplasmic reticulum-tethered transcription factor cAMP responsive element-binding protein, hepatocyte specific, regulates hepatic lipogenesis, fatty acid oxidation, and lipolysis upon metabolic stress in mice. Hepatology 55(4):1070–1082.
[12] Simonson, D.C., DeFronzo, R.A., 1990. Indirect calorimetry: methodological and interpretative problems. American Journal of Physiology 258(3 Pt 1): E399–E412.
[13] Pendergast, D.R., Leddy, J.J., Venkatraman, J.T., 2000. A perspective on fat intake in athletes. Journal of the American College of Nutrition 19(3):345–350.
[14] Frayn, K.N., 1983. Calculation of substrate oxidation rates in vivo from gaseous exchange. Journal of Applied Physiology: Respiratory, Environmental & Exercise Physiology 55(2):628–634.
[15] Guerra, M.H., Yumnamcha, T., Ebrahim, A.S., Berger, E.A., Singh, L.P., Ibrahim, A.S., 2021. Real-time monitoring the effect of cytopathic hypoxia on retinal pigment epithelial barrier functionality using electric cell-substrate impedance sensing (ECIS) biosensor technology. International Journal of Molecular Sciences 22(9).
[16] Zhang, R., 2013. MNADK, a novel liver-enriched mitochondrion-localized NAD kinase. Biol Open 2(4):432–438.
[17] Iwahashi, Y., Hitoshio, A., Tajima, N., Nakamura, T., 1989. Characterization of NADH kinase from Saccharomyces cerevisiae. Journal of Biochemistry 105(4): 588–593.
[18] Miller Jr., F.J., Gutterman, D.D., Rios, C.D., Heistad, D.D., Davidson, B.L., 1998. Superoxide production in vascular smooth muscle contributes to oxidative stress and impaired relaxation in atherosclerosis. Circulation Research 82(12):1298–1305.
[19] Shihan, M.H., Novo, S.G., Le Marchand, S.J., Wang, Y., Duncan, M.K., 2021. A simple method for quantitating confocal fluorescent images. Biochem Biophys Rep 25:100916.
[20] Thibeault, S., Rautureau, Y., Oubaha, M., Faubert, D., Wilkes, B.C., Delisle, C., et al., 2010. S-nitrosylation of beta-catenin by eNOS-derived NO promotes VEGF-induced endothelial cell permeability. Molecular Cell 39(3):468–476.
[21] Derakhshan, B., Wille, P.C., Gross, S.S., 2007. Unbiased identification of cysteine S-nitrosylation sites on proteins. Nature Protocols 2(7):1685–1691.
[22] Xiao, W., Wang, R.S., Handy, D.E., Loscalzo, J., 2018. NAD(H) and NADP(H) redox couples and cellular energy metabolism. Antioxidants and Redox Signaling 28(3):251–272.
[23] de Leeuw, C.A., Mooij, J.M., Heskes, T., Posthuma, D., 2015. MAGMA: generalized gene-set analysis of GWAS data. PLoS Computational Biology 11(4):e1004219.
[24] Anstee, Q.M., Reeves, H.L., Kotsiliti, E., Govaere, O., Heikenwalder, M., 2019. From NASH to HCC: current concepts and future challenges. Nature Reviews Gastroenterology & Hepatology 16(7):411–428.
[25] Siegel, R.L., Miller, K.D., Fuchs, H.E., Jemal, A., 2021. Cancer statistics, 2021. CA: A Cancer Journal for Clinicians 71(1):7–33.
[26] Huschka, H., Mihm, S., 2021. Hepatic IFNL4 gene activation in hepatocellular carcinoma patients with regard to etiology. International Journal of Molecular Sciences 22(15).
[27] Schulze, K., Imbeaud, S., Letouze, E., Alexandrov, L.B., Calderaro, J., Rebouissou, S., et al., 2015. Exome sequencing of hepatocellular carcinomas identifies new mutational signatures and potential therapeutic targets. Nature Genetics 47(5):505–511.
[28] Zhang, R., 2015. MNADK, a long-awaited human mitochondrion-localized NAD kinase. Journal of Cellular Physiology 230(8):1697–1701.
[29] Jo, S.H., Son, M.K., Koh, H.J., Lee, S.M., Song, I.H., Kim, Y.O., et al., 2001. Control of mitochondrial redox balance and cellular defense against oxidative damage by mitochondrial NADP+-dependent isocitrate dehydrogenase. Journal of Biological Chemistry 276(19):16168–16176.
[30] Matsuzawa-Nagata, N., Takamura, T., Ando, H., Nakamura, S., Kurita, S., Misu, H., et al., 2008. Increased oxidative stress precedes the onset of high-fat diet-induced insulin resistance and obesity. Metabolism 57(8):1071–1077.
[31] Vial, G., Dubouchaud, H., Couturier, K., Cottet-Rousselle, C., Taleux, N., Athias, A., et al., 2011. Effects of a high-fat diet on energy metabolism and ROS production in rat liver. Journal of Hepatology 54(2):348–356.
[32] Pastore, A., Piemonte, F., Locatelli, M., Lo Russo, A., Gaeta, L.M., Tozzi, G., et al., 2001. Determination of blood total, reduced, and oxidized glutathione in pediatric subjects. Clinical Chemistry 47(8):1467–1469.
[33] Goodman, R.P., Calvo, S.E., Mootha, V.K., 2018. Spatiotemporal compartmentalization of hepatic NADH and NADPH metabolism. Journal of Biological Chemistry 293(20):7508–7516.
[34] Chalkiadaki, A., Guarente, L., 2012. High-fat diet triggers inflammation-induced cleavage of SIRT1 in adipose tissue to promote metabolic dysfunction. Cell Metabolism 16(2):180–188.
[35] Rodgers, J.T., Lerin, C., Gerhart-Hines, Z., Puigserver, P., 2008. Metabolic adaptations through the PGC-1 alpha and SIRT1 pathways. FEBS Letters 582(1):46–53.
[36] Austin, S., St-Pierre, J., 2012. PGC1alpha and mitochondrial metabolism–emerging concepts and relevance in ageing and neurodegenerative disorders. Journal of Cell Science 125(Pt 21):4963–4971.
[37] Imai, S.I., Guarente, L., 2016. It takes two to tango: NAD(+) and sirtuins in aging/longevity control. NPJ Aging Mech Dis 2:16017.
[38] Pawlak, M., Lefebvre, P., Staels, B., 2015. Molecular mechanism of PPAR-alpha action and its impact on lipid metabolism, inflammation and fibrosis in non-alcoholic fatty liver disease. Journal of Hepatology 62(3):720–733.
[39] Lin, J., Handschin, C., Spiegelman, B.M., 2005. Metabolic control through the PGC-1 family of transcription coactivators. Cell Metabolism 1(6):361–370.
[40] Purushotham, A., Schug, T.T., Xu, Q., Surapureddi, S., Guo, X., Li, X., 2009. Hepatocyte-specific deletion of SIRT1 alters fatty acid metabolism and results in hepatic steatosis and inflammation. Cell Metabolism 9(4):327–338.
[41] Nogueiras, R., Habegger, K.M., Chaudhary, N., Finan, B., Banks, A.S., Dietrich, M.O., et al., 2012. Sirtuin 1 and sirtuin 3: physiological modulators of metabolism. Physiological Reviews 92(3):1479–1514.
[42] Imai, S., Yoshino, J., 2013. The importance of NAMPT/NAD/SIRT1 in the systemic regulation of metabolism and ageing. Diabetes, Obesity and Metabolism 15(Suppl 3):26–33.
[43] Chang, H.C., Guarente, L., 2014. SIRT1 and other sirtuins in metabolism. Trends in Endocrinology and Metabolism 25(3):138–145.
[44] Lempradl, A., Pospisilik, J.A., Penninger, J.M., 2015. Exploring the emerging complexity in transcriptional regulation of energy homeostasis. Nature Reviews Genetics 16(11):665–681.
[45] Houtkooper, R.H., Pirinen, E., Auwerx, J., 2012. Sirtuins as regulators of metabolism and healthspan. Nature Reviews Molecular Cell Biology 13:225.
[46] Lombard, D.B., Tishkoff, D.X., Bao, J., 2011. Mitochondrial sirtuins in the regulation of mitochondrial activity and metabolic adaptation. Handbook of Experimental Pharmacology 206:163–188.
[47] Ogryzko, V.V., Schiltz, R.L., Russanova, V., Howard, B.H., Nakatani, Y., 1996. The transcriptional coactivators p300 and CBP are histone acetyltransferases. Cell 87(5):953–959.
[48] Thompson, P.R., Wang, D., Wang, L., Fulco, M., Pediconi, N., Zhang, D., et al., 2004. Regulation of the p300 HAT domain via a novel activation loop. Nature Structural & Molecular Biology 11(4):308–315.
[49] Uehara, T., Nakamura, T., Yao, D., Shi, Z.Q., Gu, Z., Ma, Y., et al., 2006. S-nitrosylated protein-disulphide isomerase links protein misfolding to neurodegeneration. Nature 441(7092):513–517.
[50] Yang, L., Calay, E.S., Fan, J., Arduini, A., Kunz, R.C., Gygi, S.P., et al., 2015. METABOLISM. S-Nitrosylation links obesity-associated inflammation to endoplasmic reticulum dysfunction. Science 349(6247):500–506.

[51] Qian, Q., Zhang, Z., Orwig, A., Chen, S., Ding, W.X., Xu, Y., et al., 2018. S-nitrosoglutathione reductase dysfunction contributes to obesity-associated hepatic insulin resistance via regulating autophagy. Diabetes 67(2):193—207.

[52] Zhao, J., Hu, L., Gui, W., Xiao, L., Wang, W., Xia, J., et al., 2022. Hepatocyte TGF-beta signaling inhibiting WAT browning to promote NAFLD and obesity is associated with let-7b-5p. Hepatol Commun 6(6):1301—1321.

[53] Yang, L., Roh, Y.S., Song, J., Zhang, B., Liu, C., Loomba, R., et al., 2014. Transforming growth factor beta signaling in hepatocytes participates in steatohepatitis through regulation of cell death and lipid metabolism in mice. Hepatology 59(2):483—495.

[54] Garvey, E.P., Oplinger, J.A., Furfine, E.S., Kiff, R.J., Laszlo, F., Whittle, B.J., et al., 1997. 1400W is a slow, tight binding, and highly selective inhibitor of inducible nitric-oxide synthase in vitro and in vivo. Journal of Biological Chemistry 272(8):4959—4963.

[55] Sebag, S.C., Zhang, Z., Qian, Q., Li, M., Zhu, Z., Harata, M., et al., 2021. ADH5-mediated NO bioactivity maintains metabolic homeostasis in brown adipose tissue. Cell Reports 37(7):110003.

[56] Deponte, M., 2013. Glutathione catalysis and the reaction mechanisms of glutathione-dependent enzymes. Biochimica et Biophysica Acta 1830(5): 3217—3266.

[57] Helander, H.M., Koivuranta, K.T., Horelli-Kuitunen, N., Palvimo, J.J., Palotie, A., Hiltunen, J.K., 1997. Molecular cloning and characterization of the human mitochondrial 2,4-dienoyl-CoA reductase gene (DECR). Genomics 46(1):112—119.

[58] Overmyer, K.A., Evans, C.R., Qi, N.R., Minogue, C.E., Carson, J.J., Chermside-Scabbo, C.J., et al., 2015. Maximal oxidative capacity during exercise is associated with skeletal muscle fuel selection and dynamic changes in mitochondrial protein acetylation. Cell Metabolism 21(3):468—478.

[59] Xiong, Y., Guan, K.L., 2012. Mechanistic insights into the regulation of metabolic enzymes by acetylation. The Journal of Cell Biology 198(2):155—164.

[60] Hirschey, M.D., Shimazu, T., Goetzman, E., Jing, E., Schwer, B., Lombard, D.B., et al., 2010. SIRT3 regulates mitochondrial fatty-acid oxidation by reversible enzyme deacetylation. Nature 464(7285):121—125.

[61] McInnes, J., 2013. Mitochondrial-associated metabolic disorders: foundations, pathologies and recent progress. Nutrition and Metabolism 10(1):63.

[62] Gray, J.P., Alavian, K.N., Jonas, E.A., Heart, E.A., 2012. NAD kinase regulates the size of the NADPH pool and insulin secretion in pancreatic beta-cells. American Journal of Physiology. Endocrinology and Metabolism 303(2):E191—E199.

[63] Cunarro, J., Casado, S., Lugilde, J., Tovar, S., 2018. Hypothalamic mitochondrial dysfunction as a target in obesity and metabolic disease. Frontiers in Endocrinology 9:283.

64 Murray, G., Bais, P., Hatton, C., Tadenev, A.L.D., Hoffmann, B.R., Stodola, T.J., et al., 2022. Mouse models of NADK2 deficiency analyzed for metabolic and gene expression changes to elucidate pathophysiology. Human Molecular Genetics ddac151.

[65] Du, J., Estrella, M., Solorio-Kirpichyan, K., Jeffrey, P.D., Korennykh, A., 2022. Structure of human NADK2 reveals atypical assembly and regulation of NAD kinases from animal mitochondria. Proceedings of the National Academy of Sciences of the United States of America 119(26):e2200923119.

